HYDROTHERMAL TREATMENT OF NICKELIFEROUS LATERITE WITH FERRIC CHLORIDE SOLUTIONS

by

NORMAN DONALD HOLLINGSWORTH MUNROE

B.Sc. (Chemistry, Physics), University of Dar Es-Salaam. 1973

M.Phil (Mineral Process Engineering), University of Leeds, 1977

A THESIS SUBMITTED IN PARTIAL FULFILMENT OF

THE REQUIREMENTS FOR THE DEGREE OF

MASTER OF SCIENCE

in

THE FACULTY OF GRADUATE STUDIES

The Department of Metallurgical Engineering

We accept this thesis as conforming

to the required standard

THE UNIVERSITY OF BRITISH COLUMBIA

October, 1981

In presenting this thesis in partial fulfilment of the requirements for an advanced degree at the University of British Columbia, I agree that the Library shall make it freely available for reference and study. I further agree that permission for extensive copying of this thesis for scholarly purposes may be granted by the head of my department or by his or her representatives. It is understood that copying or publication of this thesis for financial gain shall not be allowed without my written permission.

Department of METALLURGICAL ENGINEERING

The University of British Columbia
2075 Wesbrook Place
Vancouver, Canada
V6T 1W5

Date 18th. NOV. 1981

ABSTRACT

The extraction of nickel and cobalt, from nickeliferous laterite, together with the hydrothermal precipitation of hematite has been investigated. In order to emphasize the relevance and significance of this process, an appraisal is made of the state of the nickel, cobalt and iron industries. A compilation of the annual production of the respective ores on the world market is included with an examination of the future uses and demand of nickel and cobalt.

Solubility relationships for iron (III) compounds in aqueous solution are reviewed in terms of pH, solution composition and temperature. The thermodynamic data used at elevated temperatures between 60°C (333°K) and 200°C (473°K) have been estimated by using the "Entropy correspondence principle" method of Criss and Coble. A sample calculation is shown in Appendix A.

The effects of (a) temperature; (b) ferric chloride concentration, (c) hydrochloric acid concentration and (d) pulp density were studied in order to evaluate extraction conditions. Generally, metal extraction increased with temperature and ferric chloride concentration. At 423°K, over 90 percent of the nickel was extracted with a ferric

chloride concentration greater than 1M. Since appreciable amounts of gangue dissolved under most conditions, thereby consuming acid, a discussion on the recovery of hydrochloric acid is presented.

Filtration of the precipitated hematite has proved difficult, because of the very fine nature of the particles. An overview of the nucleation and growth of particles in supersaturated solutions has therefore been included. This phenomenon is used to describe the phase changes which occurred during leaching experiments, and to propose an approach by which coarser particles might be achieved.

TABLE OF CONTENTS

Chapter | Page

LIST OF TABLES

LIST OF FIGURES

ACKNOWLEDGEMENTS

I am particularly indebted to my Supervisor Dr. E. Peters for his supervision, keen interest and constructive criticism of this report. I sincerely thank him, not only for his continuous guidance in matters of an academic nature but spiritual as well.

Special mention must be made of my wife, Eleise, who gave me moral support and inspiration when difficulties arose; and believe me, there were many.

Thanks are also extended to all members of the Department of Metallurgical Engineering for their cooperation and unending assistance.

The author is grateful to the National Research Council of Canada for financial support in the form of a Research Assistantship.

Chapter 1

INTRODUCTION

1.1 General

The majority of the world's known and anticipated reserves of nickel ores are lateritic deposits. Nickeliferous limonites, which constitute one of three zones of a typical laterite deposit, are also future sources of cobalt, chromium and iron.

Laterites are near-surface deposits of oxidized material formed by extreme weathering (or "laterization") of parent ultramafic rock. In contrast, the majority of the world's present production of refined nickel is from primary sulphide deposits, which tend to extend deep into the earth. Although sulphide ores are relatively easy to process (usually by a combination of ore-dressing and pyrometallurgical techniques), mining costs are escalating and established mines are getting deeper and obtaining lower grade ore. Laterites, however, are quite abundant and are much less expensive to mine.

It is an established fact that processing costs for laterites are higher than sulphide ores, because of the

necessity of chemical and/or thermal treatment of the entire ore. However, improved processing technology, increased world demand for nickel, and depleting sulphide reserves, indicate the future importance of laterite ores.

At present, this material is being treated for nickel and cobalt recovery at Nicaro and Moa Bay, Cuba,[1] and a number of new installations are projected for Australia, Indonesia, New Caledonia and the Philippine Islands. Although the mineralogy and chemical composition of materials from these countries show striking similarities, the methods used for the extraction of nickel and other desired metal values can be quite different. Those which are in commercial operation around the world include, pressure acid leaching, matte smelting, production of ferronickel in an electric or blast furnace, and selective reduction roast/ammoniacal leach.[2]

The object of this report is to investigate the chemistry of leaching nickeliferous laterite with ferric chloride solutions. In light of the fact that most of the nickel present in laterites occur in solid solution with goethite, hydrothermal treatment of the ore is a useful method of separating its metal values. Using appropriate techniques, nickel and cobalt can be recovered from the leach solution. Iron, on the other hand, is hydrolyzed to hematite and is referred to as the iron residue.

1.2 Mineralogy of Laterite Ore Deposits

All laterites are formed by weathering of the parent rock in areas of abundant rainfall. Deposits are therefore found in tropical or subtropical regions, although some laterite deposits are known to exist in more temperate zones. The nickel in the ultramafic rock usually occurs as an ion replacement in the silicate lattice or as an associated sulphide. Surface waters containing carbon dioxide leach nickel out of the ultramafic rock, carrying it downward. Reprecipitation of the metal deeper in the ore deposit may cause an enrichment of nickel in the range of 5 to 20 times the content of the parent rock.

Magnesia and silica may be leached from the parent rock, leaving varying concentrations of nickel, cobalt, chromium, iron and aluminium in the residual surface mantle. The end result of the "laterization" process is the formation of three distinct zones overlying each other and varying in chemical and mineralogical composition. Figure 1.1 depicts the variation in chemical composition and ore type with depth for a typical deposit.[3,4]

The three zones of a typical laterite deposit are: the leached or canga zone, the iron oxide or limonitic zone, and the saprolitic or magnesium-silicate-rich zone. Below the

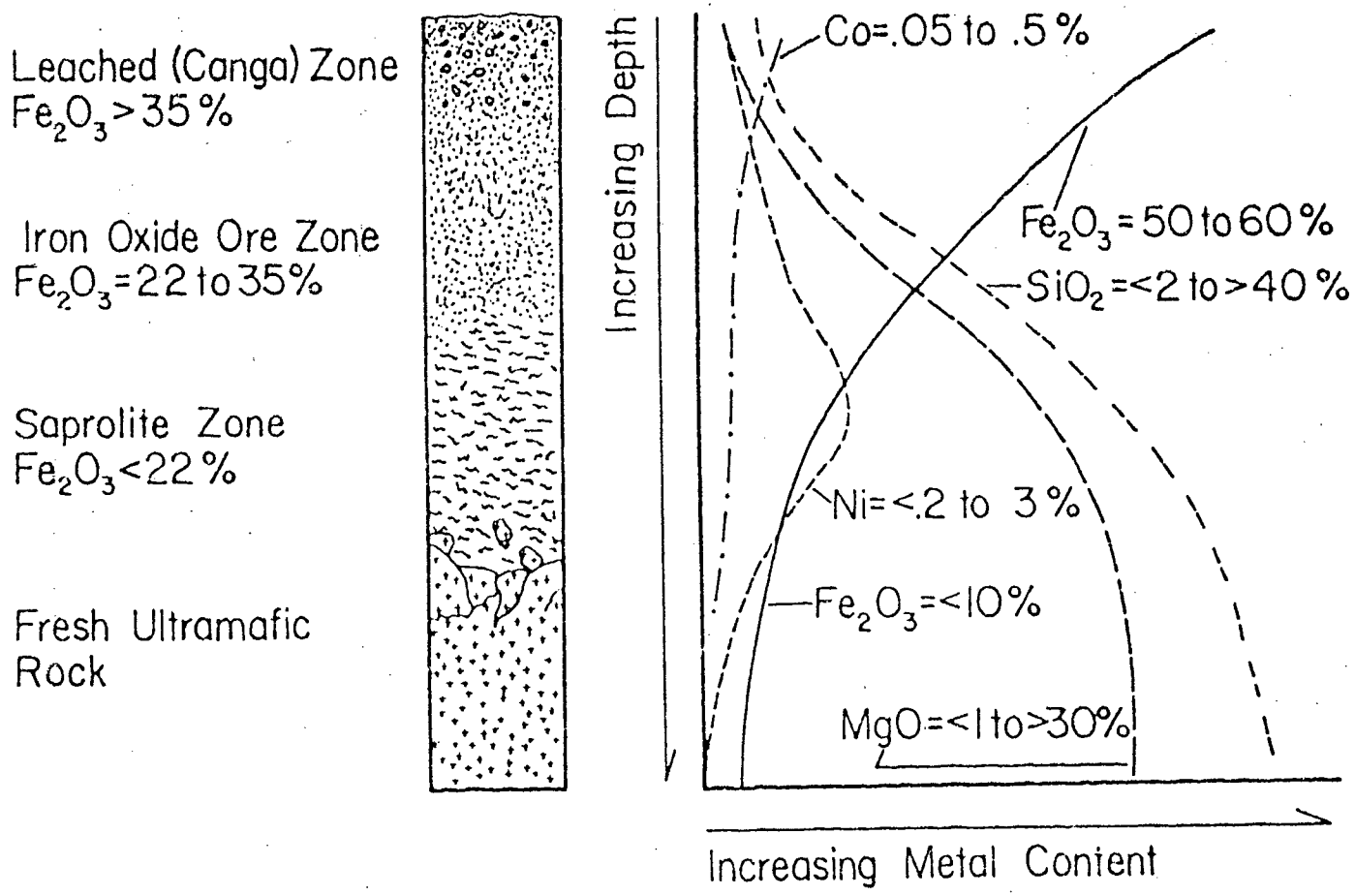

Figure 1: Chemical composition of nickel laterite ore zones.

saprolitic zone lies the remaining unaltered parent rock. Any of the three zones may be extremely thin or absent, while the thickness of individual zones may vary as much as 30-plus meters. Some deposits may even be composed entirely of almost one zone.

1.2.1 Definition and Nature of Nickeliferous Limonites

The term nickeliferous limonite[5] is used to designate the iron oxide rich zone of a laterite deposit. It consists of a cryptocrystalline mixture of goethite, with minor amounts of other hydrous oxides. Hematite, maghemite and chromite are accessory minerals commonly present, along with varying subordinate amounts of nickeliferous phyllosilicates of the montmorillonite and serpentine type. The presence of silicates has a significant impact on the efficiency of the extractive procedures, even though they contain less than a tenth of the total nickel.

Most limonites contain at least 90 percent goethite. Three-quarters of the ore's nickel and half of its chromium content occur in solid solution with the iron minerals. However, more than 90 percent of the cobalt occurs in association with manganese oxides.

The only specific nickel mineral detected in laterites

is garnierite. Investigation has shown the presence of up to an equivalent of 15 mol percent diaspore, and considerable amounts of adsorbed water. The latter is released upon heating between 383°K and the temperature of dehydroxylation - 685°K.[6]

Nickeliferous limonites analyze typically in the range 0.8 - 1.5 percent nickel, 0.1 - 0.2 percent cobalt, 1.5 - 3.0 percent chromium and 45 - 50 percent iron. In addition to nickel and cobalt, these ores are obviously important as a source of chromium and iron. All four metals should therefore be considered as potential market products.

Table 1.1 shows the distribution of major elements in nickeliferous limonites.

1.3 Economics, Market Survey and Mine Production of Nickel

1.3.1 State of the Nickel Industry

Salient statistics have revealed how vital nickel is to the iron and steel industry and the key role it has played in the development of the current aerospace industry. Nickel's greatest value is in alloys with other elements, where it adds strength and corrosion resistance over a wide range of temperatures.

Table 1.1 Distribution of Major Elements in Nickeliferous Limonites

		Content Percent	Distribution Percent
NICKEL			
Goethite	α-FeOOH	0.5 - 2	75 - 95
Manganese Oxides		4 - 20	5 - 15
Maghemite	γ-Fe_2O_3	0.2 - 1	2 - 15
Silicates		2 - 5	1 - 5
COBALT			
Manganese Oxides		4 - 20	80 - 100
Maghemite		0 - 0.3	0 - 20
CHROMIUM			
Goethite		1	50 - 70
Spinel		10 - 30	30 - 50
IRON			
Goethite		50	90+

Until 1870, nickel production was limited to small deposits in China, Germany, Greece, Italy, Norway, Sweden and the United States.[7] A nickel silicate ore was discovered in New Caledonia in 1864 by Garnier, after whom the mineral garnierite was named. New Caledonia was the principal source of nickel from 1875 until 1905, when Canada became the leading producer.[2] The Sudbury area of Canada has remained the principal source of nickel in the world.

In 1977, the main nickel industries in market economy of the free world, were located in Canada, New Caledonia and Australia (see Table 1.2). International Nickel Company of Canada, Ltd. (INCO) operated 15 mines in Canada, with several on standby. The firm also operated ore concentrators, smelters and refineries in Canada, as well as a nickel carbonyl refinery in Clydach, Wales, and a large integrated rolling mill at Huntington, West Virginia.

Falconbridge Nickel Mines Ltd. operated mines, concentrators and smelters in Ontario and Manitoba. Smelted matte was shipped to the firm's refinery at Kristiansand, Norway. At this facility, cathode nickel, nickel plating anodes and nickel sulphate were produced along with other associated metals.

Sherritt Gordon Mines Ltd. presently operates a refinery

Table 1.2 Principal World Nickel Producers

Country	Company	Nickel Products
Australia	Western Mining Corp. Ltd.	Nickel metal and matte.
	Queensland Nickel Pty.	Nickel oxide and mixed nickel-cobalt sulfides.
Bostwana	Bostwana R.S.T.	Nickel-copper-cobalt matte.
Canada	INCO, Ltd.	Nickel oxide sinter, soluble nickel oxide, nickel metal (cathode and pellets), utility shot and pig.
	Falconbridge Nickel Mines Ltd.	Nickel-copper matte.
	Sherritt Gordon Mines Ltd.	Nickel metal.
Cuba	Cubanique (State owned)	Nickel oxide and sulphide.
Dominican Republic..	Falconbridge Dominicana C. Por A	Ferronickel.
France	Société Metallurgique le Nickel (SLN)	Nickel metal, oxide, salts.
Greece	LARCO-Société Miniere el Metallurgique de Larymna S.A. ..	Ferronickel.
Guetamala	Exploraciones y Explotaciones Mineras Izabel (Inco Ltd.).	Nickel matte.
Indonesia	P.T. International Nickel Indonesia (Inco Ltd.)	Nickel matte.
	P.T. Aneka Tambang	Ferronickel.
Japan	Shimura Kako Co. Ltd.	Nickel metal.
	Sumitomo Metal Mining Co.	Nickel metal.
	Shimura Kako Co. Ltd.	Ferronickel.
	Sumitomo Metal Mining Co.	Ferronickel.
	Nippon Yakin Kogyo Co. Ltd.	Ferronickel.
	Nippon Yakin (Showa Denko)	Ferronickel.
	Nippon Mining Co. Ltd.	Ferronickel.
	Nippon Mining Co. (Hinode)	Ferronickel.
	Pacific Metals Co. Ltd.	Nickel oxide.
	Nippon Nickel	Nickel oxide.
	Tokyo Nickel	Nickel oxide.
New Caledonia	Société Metallurgique le Nickel (SLN)	Ferronickel shot, matte.
Norway	Falconbridge Nikkelverk A/S	Nickel metal.
Philippines	Mannduque Mining Corp.	Nickel briquets, powder, nickel-cobalt sulfides.
South Africa	Rustenburg Platinum Mines Ltd.	Nickel metal.
	Matte Smelters Pty. Ltd.	Nickel matte.
United Kingdom	INCO, Ltd.	Nickel metal and nickel-cobalt salts.
United States	Hanna Nickel Smelting Co.	Ferronickel.
	AMAX Nickel Division, AMAX, Inc.	Nickel briquets and powder.
U.S.S.R.	State owned	Nickel metal and matte.

at Fort Saskatchewan, Alberta, using imported nickel materials and high grade concentrates from INCO's Mine in Thompson Manitoba, after the former company shut down its Lynn Lake mine in 1977.

In countries with centrally controlled economies, the U.S.S.R. produced 80 percent of all nickel output. The nickel laterite mines in Cuba reportedly produced most of the rest.

The principal nickel producer in New Caledonia in 1977 was Société Metallurgique Le Nickel, S.A. (SLN). The company operated mines and a ferronickel smelter at Doniambo. In the past, SLN together with Le Syndicat Indépendant Des Mines have exported large tonnages of nickel ore to Japan.

Western Mining Corporation Ltd. was the largest producer of nickel in Australia during 1977. In Western Australia the firm operated several mines and a concentrator at Kambalda, a smelter at Kalgoorlie and a refinery at Kwinana. Installation of a new high capacity shaft smelting furnace was completed in late 1978. Since then, the company has exported nickel matte and concentrate to Japan.

Table 1.3[8] lists the 1977 nickel production and projected capacities by country. As is shown, 25 percent of all nickel production was derived from nickel laterites whilst 80 percent

Table 1.3 World Nickel Mine Production, 1977, and Capacity 1977, 1978, and 1980 (Thousands Tons)

	Production in 1977	Capacity		
		1977	1978	1980
North America:				
United States	13.7	18	18	16
Canada	259.4	275	275	275
Total	273.1	293	293	291
Central America and Caribbean Islands:				
Cuba	40.6	42	42	52
Dominican Republic	26.7	37	37	37
Guatemala	--	--	10	14
Total	67.3	79	89	103
Europe:				
Poland	3.1	3	3	4
U.S.S.R.	158.0	170	170	210
Other[1]	21.4	50	50	70
Total	182.5	223	223	284
Oceania:				
Australia	94.5	95	95	115
New Caledonia	120.2	150	150	170
Total	214.7	245	245	285
Asia:				
Indonesia	15.4	29	29	70
Philippines	16.5	35	35	55
Total	31.9	64	64	125
Africa:				
Botswana	13.3	20	20	20
Rhodesia, Southern	17.6	17	17	22
South Africa, Republic of	25.4	25	25	28
Total	56.3	62	62	70
Other	25.2	25	25	75[2]
World Total	851.0	991	1,001	1,233

[1]Western Europe, principally Greece and Yugoslavia.

[2]Most expansion will occur in Central and South America.

of world resources, exclusive of seabed nodules, are contained in laterites.

1.3.2 Marketed Nickel Products

Primary nickel is marketed in the form of nickel cathodes, powder, briquets, rondelles, pellets, ingots, metal shot, nickel oxide sinter and ferronickel. The chemical compositions of commercially produced primary nickel forms are given in Table 1.4.[8] Commercial nickel in these forms is normally more than 99.5 percent pure except for ferronickel and nickel oxide sinter.

The ferronickel produced in the United States contains 40 to 50 percent nickel and is sold in 50-pound pigs, whereas that produced in other countries contains 20 to 38 percent nickel. Nickel oxide sinter contains 76 percent nickel. A new product, incomet, introduced in 1974, contains 94 to 96 percent nickel and has replaced the 90 percent nickel oxide sinter introduced in Canada, but now produced only by Queensland nickel proprietary in Australia.

The availability of carbonyl pellets was greatly increased with the start up of INCO's Canadian Copper Cliff Nickel Refinery in 1974. Demand for this form of nickel has increased due to its high purity (99.97 percent), ease of handling and storage.

Table 1.4 Commercial Forms of Primary Nickel

	Composition, percent								
	Ni	C	Cu	Fe	S	Co	O	Si	Cr
Pure unwrought nickel:									
Cathode	99.9	0.01	0.005	0.002	0.001	---	---	---	---
Pellets	99.97	.01	.0001	.0015	.0003	0.00005	---	---	---
Powder	99.74	.1	---	.01	.001	---	0.15	---	---
Briquets	99.9	.01	.001	.002	.0035	.03	---	---	---
Rondelles	99.25	.022	.046	.087	.004	.37	.042	---	---
Ferronickel[1]	[2]20-50	1.5-1.8	---	Balance	.3	(2)	---	1.8-4	1.2-1.8
Nickel oxide	76.0	---	.75	.3	.006	1.0	Balance	---	---
Nickel salts:[3]									
Nickel chloride	24.70	---	---	---	---	---	---	---	---
Nickel nitrate	20.19	---	---	---	---	---	---	---	---
Nickel sulfate	20.90	---	---	---	---	---	---	---	---

[1]Ranges used to denote variable grades produced.

[2]Cobalt (1 to 2 percent) included with nickel.

[3]Theoretical nickel content.

1.3.3 State of the Nickel Market

Sharp swings in nickel deliveries and refined production have occurred since 1967. A significant buildup of producer inventories during 1975-1977 was followed by a steep decline in 1978-1979. However, during 1981 a modest increase in producer inventories is anticipated.

The short and drastic swings in consumption patterns are illustrated in the following charts. See Figures 1.2, 1.3 and 1.4.[9] Recent market studies suggest that the historical growth in nickel consumption of 6 percent per year began to weaken in 1975-1976. It is now estimated that 4 percent per year is a reasonable yardstick for growth expectations through 1985 and possibly in 1990. The 4 percent trend assumes that the rate of capital spending will be stimulated, and that increased utilization of nickel will occur in energy programs associated with coal processing, oil and gas drilling and the development of the nickel-zinc battery.

1.3.4 Prices

In 1980, INCO introduced a temporary 6 percent across-the-board discount from published prices for competitive reasons. Further price erosion is not expected for the following reasons:

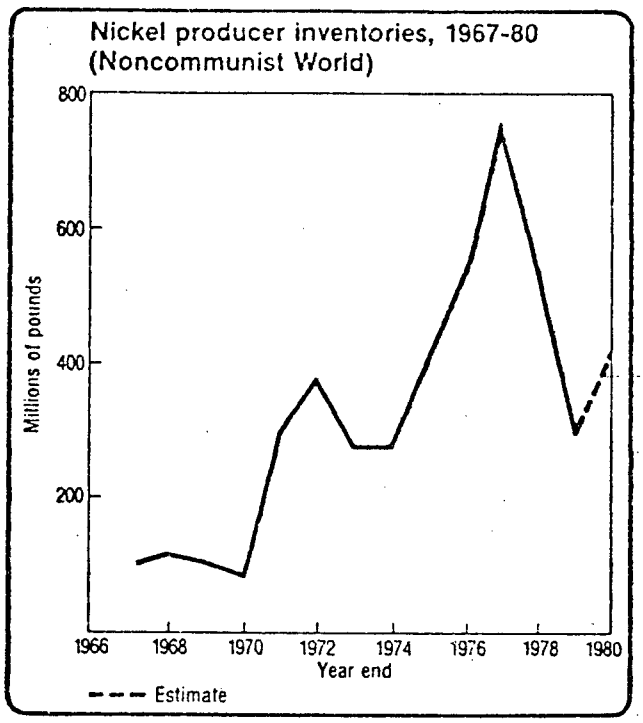

Figure 1.2 Nickel producer inventories, 1967-1980 (Noncommunist World).

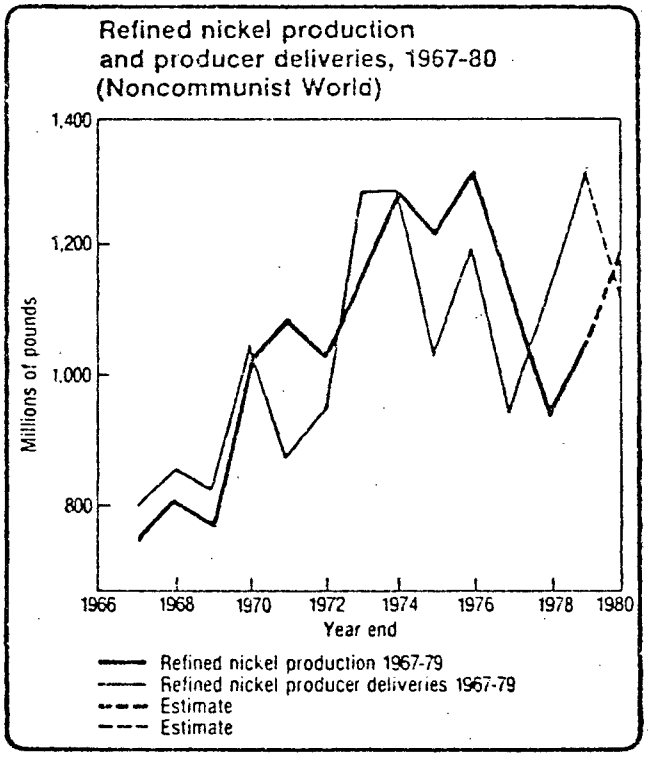

Figure 1.3 Refined nickel production and producer deliveries, 1967-80 (Noncommunist World).

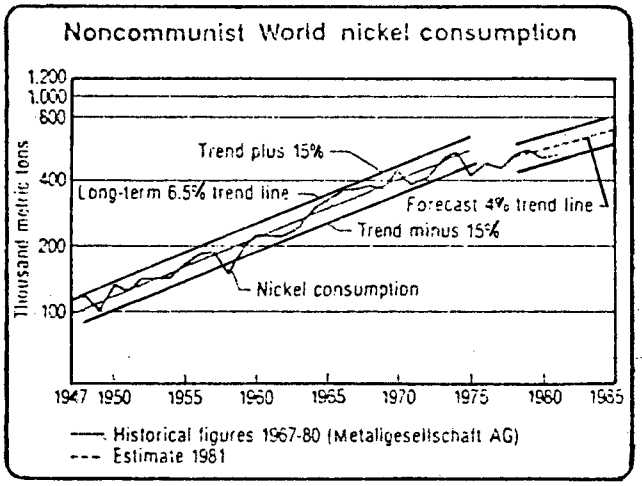

Figure 1.4 Noncommunist World nickel consumption.

1) Producer inventories will be maintained at more reasonable levels and consumer inventories now stand at a low level.

2) Production cutbacks have been initiated by the major producers in order to keep inventories in line with demand.

3) Production costs have continued to escalate sharply. Nickel products derived from laterite ores (which account for about 45 percent of non-communist world production) are under special cost pressure. At certain laterite based facilities, energy costs are 50-60 percent of the total production cost.

4) Under present economic circumstances, the published price of $3.45 (U.S.) per pound does not yield an adequate return on investment.

Over the longer term however, nickel markets face an impressive building of latent demand in the energy and transportation sectors. Normal levels of nickel consumption are anticipated through 1982, by which time, some of the currently idle standby capacity may be required. In other words, the current market weakness has not yet run its course, but optimism and confidence are growing, now that stronger demand lies ahead.

1.3.5 Resources - Reserves of Nickel

Total identified resources of nickel have been estimated at 230 million tonnes, whilst world nickel reserves were 60 million tonnes.[8]

A report from the U.S. Geological Survey[10] indicated that the combined sulphide and laterite world resource was approximately 7 billion tonnes averaging about 1 percent nickel. This figure appears to be very modest, because counting only deposits in countries bordering on the Caribbean and Islands of the Western Pacific, the tonnage of nickeliferous laterites analysing more than 0.8 percent nickel and averaging about 0.1 percent cobalt, amounts to at least 10 billion tonnes.[11]

1.3.6 Uses

In 1979, pure unwrought nickel constituted 68 percent of the total primary nickel market; ferronickel, 20 percent; and nickel oxide sinter, 11 percent.[8] The pure forms were utilized mainly in the production of nickel wrought products, high-nickel heat and corrosion-resistant alloys, copper-base alloys and in electroplating, whereas ferronickel and the oxide sinter were used largely in the production of stainless and alloy steels.

Table 1.5 Identified World Nickel Resources (Thousand Tons)

	Reserves	Other Resources[1]	Total Resources[1]
North America:			
United States	200	14,900	15,100
Canada	8,700	12,500	21,200
Total	8,900	27,400	36,300
Africa	2,300	6,700	9,000
Central America and Caribbean Islands:			
Cuba	3,400	14,200	17,600
Dominican Republic	1,100	100	1,200
Guatemala	300	900	1,200
Puerto Rico	---	900	900
Total	4,800	16,100	20,900
Europe: U.S.S.R.	8,100	13,200	21,300
Oceania:			
Australia	5,600	3,200	8,800
Indonesia	7,800	55,000	62,800
New Caledonia	15,000	31,000	46,000
Philippines	5,700	10,600	16,300
Total	34,100	99,800	133,900
South America:			
Brazil	460	3,640	4,100
Colombia	900	600	1,500
Venezuela	---	700	700
Total	1,360	4,940	6,300
World total (rounded)[2]	60,000	168,000	228,000
World total, seabed nodules[3]	---	760,000	760,000

[1] Derived in consultation with U.S. Geological Survey and revised March 1978.

[2] Excludes nickel associated with seabed manganese nodules.

[3] Based on Holser, 1975 paramarginal resource estimate of 76 billion dry short tons of sea nodules and the NMAB-323, 1976 estimate of average nodule composition of 1 percent copper, 1 percent nickel, 24 percent manganese, and 0.35 percent cobalt.

The approximate current use pattern of nickel is shown below:

Uses	Percentage of All Nickel
Stainless steels	41
Nickel plate	16
High nickel alloys (monels, coinage)	12
Nimonic alloys (60% Ni), Cr, Fe	10
Iron and steel castings	9
Copper and brass products	3
Others (batteries, magnets, catalysts)	9
	100

1.4 Economics, Market Survey and Mine Production of Cobalt

1.4.1 State of the Cobalt Market and Industry

World cobalt production from primary sources in 1980 remained unchanged from the previous year at 26,000 tonnes. Secondary production increased to 1,000 tonnes, up 20 percent. However, real consumption fell as much as 15 percent below the 1979 level. Moreover, as a result of destocking, the apparent consumption fell by as much as 35 percent. It is generally felt that the combined effects of lower consumption, increased substitution and unprecedented destocking reversed the world cobalt demand equation for 1980.

Cobalt's use in high performance services practically guarantees its continued growth in demand, regardless of high prices. There are two areas in which cobalt seems to be relatively immune to substitution in the time horizon of ten to twenty years. These are super alloys and catalysts. Super alloys are primarily used in three major growth areas:

1) Turbines and jet engines.
2) Surgical implants.
3) Oil field goods.

In applications where the high temperature performance is crucial, properties imparted by cobalt are so valuable that the price is less important than long-term availability.

The second most important metallurgical use of cobalt is in magnets. Permanent magnets of the alnico variety, which exhibit excellent magnetic properties, have traditionally been a large consumer of cobalt. Recently, however, this demand for the metal has been declining due to the advent of hard ferrites as a substitute. The approximate current use pattern of cobalt is shown in Table 1.6.

1.4.2 Resources - Reserves of Cobalt

Most cobalt resources are only available as by-products of mining for more abundant elements. Only the

Table 1.6 Western World Cobalt Market Consumption Shares (Percentage)[9]

	1970	1980	1990[1]
Magnetic Alloys	20	16	17
Cemented Carbides	5	7	8
Superalloys and Other Alloys	45	47	40
Ceramics and Enamel	12	10	8
Chemicals	18	20	27

[1]Estimated

Moroccon Bouazzer deposit is of a high enough grade to necessitate production of cobalt as the principal metal.

Much of the world's identified resources are in the form of lateritic nickel ores in tropical regions, such as the Philippines, Indonesia and New Caledonia. Australian production from laterites has become an increasingly significant source as has the Cuban. Nevertheless, most cobalt currently comes from sulphide and oxide deposits in Zaire, Zambia, Finland and Canada.

Reserves

It has been estimated that the world's continental resources amount to some 9 million tonnes of cobalt. An estimation by country is outlined as follows:

Zaire	3,090,000 tonnes
Zambia	1,704,000 tonnes
Cuba	1,049,000 tonnes
USA	764,000 tonnes
Canada	249,000 tonnes

Of these resources, the estimated reserves are:

Zaire	1,520,000 tonnes	42%
Zambia	699,000 tonnes	19%
Canada	20,000 tonnes	0.5%

from a total reserve of 3,618,000 tonnes. To this can be added a further 12 million tonnes resource hoistable from the sea bed.

Thus, it can be seen that Zaire and Zambia possess 53 percent of the known land resource and 61 percent of the proven reserves.

1.4.3 Production of Cobalt

The significance of these reserves has been translated into production and the contribution of Central Africa is as follows:

During the period 1925-1975 Zaire produced 947,500 tonnes

1933-1975 Zambia produced 51,993 tonnes

and more recently:

	Zaire (tonnes)	Zambia (tonnes)	Canada (tonnes)	World (tonnes)
1976	10,700	1,700	1,900	17,400
1977	10,200	1,700	1,400	17,435
1978	12,300	1,800	1,450	20,090
1979	12,000	3,000	1,600	21,800
1980	13,400	3,000	-	23,214

Hence, the Central African source is established as the producer of some 70 percent of the world's cobalt.

1.5 Iron Ore - Market Relevance to Iron Residue

1.5.1 The State of Steel Production

World steel production, which had been advancing annually since 1977, was projected by the International Iron and Steel Institute (IISI), to fall by 4 percent in 1980 to 717.7 million tonnes. This was primarily due to a state of recession in the iron and steel industry in North America and Europe. However, decline is not the whole picture, because there is an anticipated increase in steel output of about 2.2 percent in eastern bloc countries, and 3.6 percent in developing countries.

It was expected that three countries would record significant production increases in 1980. Italy up by about 9.8 percent, Brazil up by about 10.7 percent and South Korea up by 13.1 percent over the 1979 figures.

1.5.2 The Role of the Iron Residue from Nickel-Laterites in the Direct Reduction of Iron (DRI) Industry

Despite a rather uncertain start with regards to scaled up commercial operations, 12 direct reduction iron processes had been applied commercially throughout the world by the end of 1979 (see Table 1.8).

Table 1.7 World Raw Steel Production by Region (Million Tonnes)

	1977	1978	1979	Projected 1980	Percentage Change 1979-1980
World	708.8	712.5	747.4	717	- 4.0
U.S.	132.2	123.8	123.3	100.8	-18.2
Japan	117.1	102.1	111.7	111.8	0
E.E.C.	155.6	132.4	140.0	128.4	- 8.2
Developing Countries	31.1	46.6	55.6	57.6	+ 3.6
Eastern Europe	185.1	211.9	209.4	214.4	+ 2.2

Source: International Iron & Steel Institute.

Table 1.8 Direct-reduced Iron Processes Applied Commercially at Year-end 1979

Process	Type and Equipment	Reductant	Product
Hyl	Batch	Gas	Sponge iron, lump, or pellets.
	Retort		
	Vertical Shaft	Gas	Sponge iron or lump.
Hoganas	Saggers in tunnel kiln	Coal or coke	Sponge iron or metal powder.
	Shaft	Gas	Lump or pellets.
	Shaft	Gas	Lump or pellets.
High-iron briquets(HIB)	Fluid bed	Gas	Iron briquets.
SL/RN	Rotary kiln	Coal or coke	Lump, pellets, fines, or briquets.
Kinglor-Metor	Rotary kiln	Coal or coke	Lump or pellets.
Esso (FIOR)	Fluid bed	Gas	Briquets
Purofer	Shaft	Gas	Lump or pellets.
Krupp	Rotary kiln	Coal	Sponge iron.
-Chalmers (ACCAR)	Rotary kiln	Coal/oil/gas	Sponge iron.
Nippon Steel[1]	Rotary kiln	Coal or coke	Pellets.
Sumitomo[1]	Rotary kiln	Coal or coke	Pellets.
Kawasaki[1]	Rotary kiln	Coke breeze	Pellets.

[1]Designed to produce sponge iron from waste materials accumulated at integrated steel plants.

The importance of direct-reduced iron (DRI) in the world's steel industry is reaching new heights, as demonstrated by the rapid growth of plant capacities in the past 10 years (see Table 1.9). During the 11-year period 1970-1980, DRI capacity has increased over 970 percent to 20.46 million tonnes per year. It is anticipated that new plants currently under construction should take capacity to over 31.0 million tonnes by 1982.

The U.S.S.R. remains the world's leader in steel production with an estimated output of 152 million tonnes in 1980, which was up 1.9 percent above the 1979 figure. Japan showed an output of 111.8 million tonnes in 1980, which was almost identical to the 1979 level. However, the final figures for the U.S., the world's third largest steel producer, revealed a decline of approximately 18.2 percent in 1980 output.

The greatest concentration of DRI production is located in developing countries, where electric-arc steel making, with its low investment cost, is very popular. DRI is attractive in such nations because they do not have good sources of scrap for supplying iron units to their electric furnaces. There is also a growing interest in DRI among developed countries as a means of diluting the undesirable residual elements which contaminate their scrap supplies. Finally, a concern of many steel producers in countries, such as the U.S., is that the

Table 1.9 Growth of World DRI capacity (Tonnes)

Year	Capacity
1970	1,906,000
1971	2,754,000
1972	3,324,000
1973	4,650,000
1974	5,775,000
1975	6,650,000
1976	7,810,000
1977	10,775,000
1978	14,325,000
1979	17,625,000
1980	20,460,000

rapidly growing number of electric-arc furnaces will raise the demand and price of scrap beyond economical limits. All of these factors contribute to the high level of interest in DRI.

The DRI process can be classified into those that require high-grade iron ore or agglomerates with strict limitations on impurities, or those that can reject the impurities to produce a high-grade concentrated product. It is anticipated that in the former case treated iron residue could meet acceptable specifications with regard to nickel, chromium, and alumina for utilization in a DRI process.

1.5.3 Outlook for the Future Use of the Iron Residue

The future utilization of chemically treated iron residue from nickel laterites in DRI processes appears promising for the following reasons:

1) The DRI processes should continue to rise in popularity throughout the world as increased use is made of electric-arc furnaces.

2) The greatest concentration of DRI production will be located in developing countries, where electric-arc steel making, with its low investment cost, is very popular.

3) The U.S. and other developed nations have embarked on a policy of helping developing countries help themselves.

4) The largest known terrestial reserves of nickiliferous laterites occur in developing countries and in some instances close to existing Bauxite Industries.

5) By-product caustic from the Bayer process can be employed for chromium extraction from the leached ore.

1.6 Review of Existing Methods of Nickel Extraction From Laterites

1.6.1 Laterite Processing Methods - General

There are several commercial alternatives that exist for the extraction of nickel from nickel laterite ores. The choice of the extraction process employed, however depends on several factors such as:

1) The physical and chemical nature of the ore body.

2) The geographical location, which is directly related to supply and cost of necessary raw materials and energy.

3) The marketability of the end products, may depend on geographical location.

Several processes for the recovery of nickel and cobalt have been described, all of which, however, show some disadvantages. Typical examples of these processes are: selective extraction with dilute acids,[13,14] selective

conversion of nickelous and cobaltous oxides with gaseous hydrogen chloride[15,16,17] and selective reduction of the above-mentioned oxides with carbon monoxide/carbon dioxide mixtures, followed by extraction with ammonia-ammonium carbonate solutions.[18]

Van Nes and Heertjes[19] later described a method of increasing the ratio of the amounts of nickel and cobalt with respect to iron. This was realized by converting nickel oxide and cobalt oxide, almost selectively and completely, into the corresponding chlorides. A step-wise process was used in which a gaseous mixture of steam and hydrogen chloride was passed through a fluidized bed of the granulated ore, under proper conditions of temperature and concentration. The chlorides were recovered by extracting the chloridized ore with hot water.

Roorda and Queneau,[11] more recently proposed a process, based on pyrometallurgical selective reduction of nickeliferous limonites, followed by aqueous chlorination in seawater. Though conducted only on a laboratory scale, process variables were kept within specific constraints, which could be imposed industrially. The methods employed were simple, flexible and amenable to economic, large scale, automated unit operations.

Significant advantages of this process include: a high recovery of nickel and cobalt of over 90 percent, the potential important source of chromium and iron due to chlorine leaching of the ore, rapid dissolution rates which minimize leaching circuit costs, the use of salt rather than fresh water and finally, the intrinsic superiority of chloride systems in solvent extraction with its attractive process economics.

The processes currently in commercial operation include: pressure acid leaching, matte smelting, production of ferronickel by electric or blast furnace and selective reduction roast/ammoniacal leach.

1.6.2 Pressure Acid Leaching

In the pressure acid leach process, finely crushed and ground ore is slurried and leached with dilute sulphuric acid at high temperature and pressure, usually in excess of 522°K and 4.1×10^{6} Newtom metre^{-2}. At these temperatures iron and aluminium form basic sulphates of low residual solubility. The resulting metal containing solution is then separated from the solid residues by means of dewatering thickners and the metal values precipitated by sulphide addition (usually hydrogen sulphide). An alternative route to product recovery is solvent extraction of the pregnant leach liquor followed by electrowinning.

Recoveries of desired metal values by acid leach processing are usually very high. Furthermore, acid leaching is not very selective. Magnesia and alumina consume excessive amounts of sulphuric acid, meaning that the feed ore must be low in these compounds or operating costs may become prohibitive. Therefore, the application of acid leaching is limited to a narrow range of ore types. It should also be noted that the basic sulphate residue is a source of environmental pollution, because of dissolution of sulphate and metal ions into run-off waters.

1.6.3 Matte Smelting

In this process, ground ore is charged to a blast furnace in the presence of coke, gypsum, and limestone. The coke is present as a reducing agent to convert nickel and iron oxides to the metals. The gypsum is reduced to calcium sulphide, which reacts with the nickel and iron to produce a metal sulphide matte. In addition to the molten matte, the high temperatures of the process result in the formation of a molten slag by the remainder of the ore and limestone. The imiscibility of the slag and matte facilitates their physical separation. The molten nickel-iron matte is then air blown in converters to oxidize the iron. Addition of silica flux produces a secondary iron-rich slag, which can be easily separated from what is now the nickel matte. Further refinement by oxidation roasting followed by reduction result in nickel metal.

Matte smelting is used on a wide variety of ores due to the inherent selectivity of the process. However, the process is very energy intensive, and may be ruled out in certain geographical locations. Sulphur dioxide gas emission is an unwanted, but unavoidable, by-product of this process.

1.6.4 Ferronickel Production

Ferronickel production is very similar to that of nickel matte production, the major difference being that no sulfidizing agent is added. As a result, the initial reduction step produces a molten crude ferronickel and silicate slag. The crude ferronickel is then usually oxidized in a converter to remove impurities such as carbon, silicon, chromium, and phosphorus in a secondary slag.

Here, a wide range of ores may be treated, but those high in silicates are desirable because of the ability to from a good primary slag. This process is very energy intensive, particularly if electric smelting is used to melt a high-silica ore (high-silica ores have higher temperatures of fusion and require the accurate temperature control that can be provided by electric furnaces).

1.6.5 Selective Reduction Roast/Ammoniacal Leach

The main objective in the selective roast/leach route is to reduce the desired metal oxides in laterite ores

to the respective metals, using a gaseous reductant and a moderately high temperature. The metals are then oxidized in an ammoniacal-ammonium carbonate solution.

The most important precaution is ensuring that the iron oxides in laterite are not reduced to a form that is soluble in the leach. This affects the oxidation and subsequent solubilization of the nickel and cobalt. Furthermore, reduction to metallic iron results in excessive consumption of costly reductants. The desired solubilized metals are recovered from solution by several established methods. Solvent extraction followed by electrowinning or hydrogen reduction is one such example.

Other reductive roast/ammonia leach processes currently in advanced stages of development, but not in commercial operation, includes the U.S. Bureau of Mines (USBM) process[20] and the UOP additive process.[3] The USBM uses ammoniacal-ammonium sulphate solution for leaching.

Chapter 2

A REVIEW OF PREVIOUS INVESTIGATIONS ON DIRECT ACID LEACHING

2.1 Direct Acid Leaching of Nickeliferous Laterites

Many leaching methods[13,14,21,22] have been proposed for obtaining nickel and cobalt from nickeliferous laterites. Although processes considered cover a wide variety of leaching procedures, they all have certain aspects in common. These are:

1) A pretreatment stage, usually reduction roasting and/or

2) high temperature-pressure leaching.

In view of escalating energy costs, many workers have concentrated their efforts on bypassing the expensive pretreatment reduction roast stage. However, most of these investigations have been on a laboratory scale, and in some cases up to the pilot plant level.

Proposed processes for direct extraction of the nickel and cobalt values without roasting include sulphuric, hydrochloric, and nitric acid leaching.[2] Due to a lack of

selectivity, and severe corrosive conditions, the use of mineral acids has so far been unsatisfactory. Similar chemical behaviour of the oxides results in mechanically complex unit operations, which may be prohibitive.

At the present writing, laboratory investigations[23] indicate that a promising process may be devised for hydrochloric acid leaching of serpentine type ores (high magnesium silicates). This was based on the fact that the relative quantities of impurities, which dissolve and consume acid, are much lower in such ores. However, there was less optimism for direct leaching of nickeliferous laterite (low magnesium).

2.1.1 Direct Leaching of Goethite

Mineralogically, the predominant mineral species present in Nickeliferous laterites is goethite (α-FeO(OH), $HFeO_2$ or $Fe_2O_3.H_2O$), with varying amounts of impurity (SiO_2 as quartz or silicate). One of the more striking features of such laterites is the extremely fine particle size of goethite. Usually, 50 percent or more of the particles is smaller than 10 µm. Due to the highly disseminated nature of such deposits, physical beneficiation of three quarters of the ore's nickel value from goethite is virtually impossible. As a result, any attempt to describe direct acid leaching of nickeliferous laterites is incomplete without considering the leaching of goethite.

Goethite has an orthorhombic structure[24,25] and is anisotropic in nature. Figure 2.1 shows its crystal structure, which is isomorphous with diaspore (α-AlO(OH)). The oxygen atoms are arranged in a hexagonally close-packed layer, with the iron atoms in octahedral interstices.

A drastic change in surface area due to pitting,[26] is known to occur with hydrochloric acid attack of goethite. Various workers[27,28,29] have shown rates of attack, which increase in the order - Perchloric acid <sulphuric acid <hydrochloric acid, when considering solutions of equal normality greater than 1N. Azuma and Kametani[30] subsequently correlated these increasing absolute rates of leaching in different acids with the increasing complexity constants of the respective anions for ferric ion.

Goethite has an activation energy for direct dissolution in various acids similar to that of hematite. Activation energies obtained for different acids are listed in Table 2.1.[26,27,28] No significant change in activation energy values with acid concentration was observed, although dissolution rates in hydrochloric acid increased sharply up to 6N. Surana[28] postulated that both goethite and hematite react by similar chemical mechanisms.

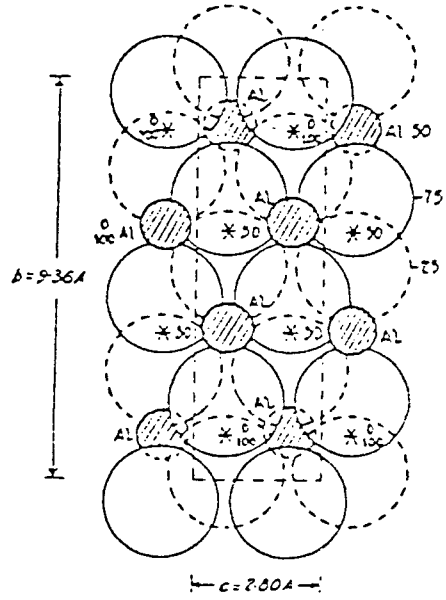

Figure 2.1 The structure of diaspore and goethite (after Bragg).

Table 2.1 Activation Energies for Direct Dissolution (Kcal/mol)

Material		ACID		
		HCl	H_2SO_4	$HClO_4$
Massive red	α Fe_2O_3	23.4	18.7 ± 2.5	
Botryoidal	α Fe_2O_3	23.2	20.2 ± 1.8	21.1 ± 5.2
Brazilian	α Fe_2O_3	22.7		
Synthetic	α Fe_2O_3	22.6	18.4 ± 2.0	22.1 ± 4.5
Goethite		21.1		
Synthetic	α Fe_2O_3	19.5 - 21.6		
Single crystal	α Fe_2O_3	20 - 24		
Goethite		22.5	19.8	
Synthetic	α Fe_2O_3	21.9	18.2	19.2 - 21.4

2.1.2 Mechanisms of Leaching of Goethite

Bath[26] proposed a mechanism by which the surface of goethite is first assumed to undergo hydration. This is believed to be rapid.

In order to describe the mechanisms, a hydrated surface will be represented by:

$$\Big|_{s}\text{-O-Fe-OH}$$

The surface may be protonated,

$$\Big|_{s}\text{-O-Fe-OH} + H_3^+O \overset{K_1}{\rightleftharpoons} \Big|_{s}\text{-O-Fe}^+ + 2H_2O$$

The anion Cl^- may be adsorbed on the surface site

$$\Big|_{s}\text{-O-Fe}^+ + Cl^- \overset{K_2}{\rightleftharpoons} \Big|_{s}\text{-O-Fe-Cl}$$

and this complex may then desorb, (rate determing step).

$$\Big|_{s}\text{-O-Fe-Cl} \xrightarrow{k_2} FeOCl_{aq.}$$

The overall reaction is:

$$\Big|_{s}\text{-O-Fe-OH} + H_3O^+ + Cl^- \longrightarrow FeOCl_{aq.} + 2H_2O$$

and the rate equation is:

$$d\frac{(Fe)_{aq.}}{dt} = K_2K_1k_2\left[\Big|_{s}\text{-O-Fe-OH}\right] a_{H^+} \cdot a_{Cl^-}$$

Ahmed and Maksimoir[32] in their study of zero point of charge of hematite in various acids, postulated that the surface may undergo protonation to form an aquo complex or be attacked directly by the anion. A dual mechanism may thus be operative.

The surface may first undergo a protonation as previously described.

$$\left|_{s}\text{-O-Fe-OH} + H_3^+O \overset{K_1}{\rightleftharpoons} \right|_{s}\text{-O-Fe}(H_2O)^+ + H_2O$$

This aquo complex may either desorb

$$\left|_{s}\text{-O-Fe}(H_2^+O) \xrightarrow{k_1} \text{O-Fe}(H_2O)^+_{aq}\right.$$

or adsorb an anion X^-

$$\left|_{s}\text{-O-Fe}(H_2^+O) + X^- \overset{K_2}{\rightleftharpoons} \right|_{s}\text{-O-Fe-}(H_2O)X$$

The resulting complex then desorbs

$$\left|_{s}\text{-O-Fe}(H_2O)X \xrightarrow{k_2} \text{O-Fe}(H_2O)X_{aq}\right.$$

Assuming once again that desorption is the rate limiting step, the overall reaction may be written

$$2\left|_{s}\text{-O-Fe-OH} + 2H_3O^+ + X^- \longrightarrow \right.$$

$$\text{O-Fe}(H_2O)^+_{aq} + \text{O-Fe}(H_2O)X_{aq} + 2H_2O$$

and the rate will be given by:

$$\frac{d[Fe]}{dt} = \frac{d[O\text{-}Fe(H_2O)^+]}{dt} + \frac{d[O\text{-}Fe(H_2O)X]}{dt}$$

$$= k_1 K_1 \left[\left|_s\text{-}O\text{-}Fe\text{-}OH \right] a_{H^+} + k_2 K_2 K_1 \left[\left|_s\text{-}O\text{-}Fe\text{-}OH \right] a_{H^+} a_{X^-} \right.$$

$$= K_1 \left[\left|_s\text{-}O\text{-}Fe\text{-}OH \right] a_{H^+} \left(k_1 + k_2 K_2 a_{X^-}\right) \right.$$

In this case, the anion Cl^- is a good complexer with iron, and K_2 will be large. As the anion will rapidly adsorb on the surface, $\left|_s\text{-}O\text{-}Fe\text{-}H_2^+O\right.$ will be low, and the rate equation is simplified to,

$$\frac{d[Fe]}{dt} = k_2 K_2 K_1 \left[\left|_s\text{-}O\text{-}Fe\text{-}OH \right] a_{H^+} a_{Cl^-} \right.$$

$$= K_\alpha a_{H^+} a_{Cl^-}$$

where $K_\alpha = k_1 K_1 K_2$ (surface sites remaining constant)

It is interesting to note that this expression is identical to that obtained previously, which is known to fit the experimental results for hydrochloric acid.

At higher HCl concentration, chloride ions may adsorb on the surface, and the equilibrium may be written:

$$\left|_s\text{-}O\text{-}Fe^+ + Cl^- \rightleftharpoons \right|_s O\text{-}Fe\text{-}Cl$$

At high enough hydrochloric acid concentration, the surface sites become saturated with anions. Dissolution may then proceed by a further protonation of the activated surface

$$\left|_{s}\text{-O-Fe-Cl} + H_3^+O \underset{}{\overset{K_3}{\rightleftharpoons}} \left|_{s}\text{OH-Fe-Cl}^+ + H_2O\right.\right.$$

This would be followed by the rate-determining desorption of the ferric ion complex

$$\left|_{s}\text{OH-Fe-Cl}^+ \xrightarrow{k_2} \text{FeOHCl}^+_{aq}\right.$$

where K_2 is the reaction rate constant.

The rate equation in strong acid solution is then:

$$\frac{d\,[Fe]_{aq}}{dt} = k_2K_3\left[\left|_{s}\text{-O-Fe-Cl}\right.\right] a_{H^+}$$

The rate of leaching now depends on K_3, which may depend on the "activation" of the surface by each anion, and this in turn could be related to the complexing power of anions for ferric ions.

2.1.3 Direct leaching of Low Magnesium Limonites

Laboratory experiments[23] involving the leaching of nickel laterite ores in hydrochloric acid have shown that the extraction of nickel and iron is closely related to the

weight of goethite dissolved. Very little extraction occurs at ambient temperatures, usually less than 10 percent. Dissolution of the goethite increases drastically from about 348°K, and complete dissolution may be expected at 423°K for a leaching time of one hour, at hydrochloric acid concentration greater than 2M.

The general conclusions are that, at low temperatures, acid concentration is the dominating factor in the percentage metal extraction. However, leaching at higher temperatures, 353°K and over, results in almost the same percentage extraction irrespective of acid concentration. However, maximum nickel extraction is only achieved with complete dissolution of the ore.

2.2 Hydrothermal Precipitation in Solutions Containing Mainly Ferric Ions

2.2.1 Hydrolysis of Metal Species at Elevated Temperatures

Very little is known regarding the hydrolysis reactions of inorganic ions at higher temperatures. This is due to a dearth of thermodynamic data for aqueous solutions in the temperature range 373 - 573°K. Many of the older data on the temperature coefficients of simple cations have been obtained before it was recognized that dimerization and

polymerization had to be considered.

The correspondence principle of Criss and Cobble[33,34] has therefore been used to more accurately predict thermodynamic equilibria at elevated temperatures. In effect, entropies and heat capacities of ionic species participating in a given reaction are utilized in computing the standard free energy changes at temperatures other than 298°K.

A useful method of presenting thermodynamic data related to the hydrolysis of metal species at elevated temperatures, is the use of temperature/pH diagrams, such as the Fe^{3+}—H_2O system shown in Figure 2.2.[35] The precipitation temperature and the composition of the precipitate formed were shown to be dependent on the pH of the initial nitrate solution. Although precipitation of hematite from ferric chloride solution is not expected to show identical behaviour, the equilibrium diagram may serve as a guide.

2.2.2 Precipitation of Iron as Ferric Oxide

An examination of the temperature versus pH plot suggests that iron can be removed from leach solutions by hydrolysis at high temperatures of about 473°K. In practice however, it has been found that in the absence of jarosite precipitants, the extent of hydrolysis[36] and precipitation of

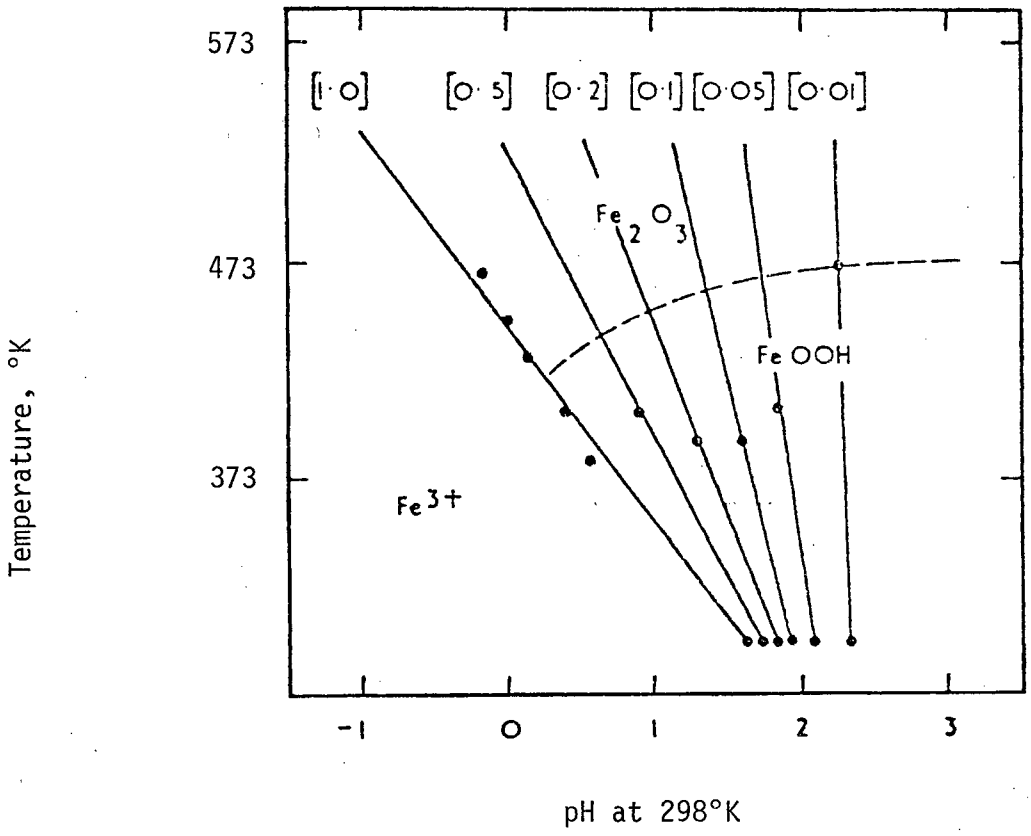

Figure 2.2 Experimental temperature vs pH_{298} diagram for the Fe^{3+}—Fe_2O_3—H_2O system.

ferric oxide at 473°K is not always sufficient for the iron content of the final solution to be lowered to a level, which is of practical importance.

There are two methods of increasing the extent of hydrolysis and precipitation of ferric oxide. One method is to heat the leach solution to well over 473°K. This however results in an increase in operating pressure, and increased corrosion problems. Alternatively, an increase in the extent of precipitation is accomplished by a decrease in the 'free acid' level of the hydrolyzed liquor.

In considering stability relations of the compounds α-Fe_2O_3, and α-FeO(OH) in aqueous solutions of Fe^{3+} at various temperatures, the general form of the precipitation reaction can be written:

$$2M^{x+} + yH_2O = M_2O_x \cdot (y-x)H_2O + 2xH^+$$

Considering the systems in the form M^{x+}—M_2O_x—H_2O leads to the possibility of representing reactions on temperature-pH plots of the type shown in Figure 2.2. The standard isotherm may be written as:

$$\Delta G_T^\circ = -RT \ln \frac{a_{M_2O_x \cdot (y-x)H_2O} \; a_{H^+}^{2x}}{a_{M^{x+}}^{2} \; a_{H_2O}^{y}}$$

and simplified to:

$$2xpH = \frac{\Delta G_T^\circ}{4.575T} - 2 \text{ Log } m_{M^{x+}} - 2 \text{ Log } \gamma_{M^{x+}}$$

The pH at which various compounds are in equilibrium with aqueous solutions of the metal ions can thus be calculated as a function of temperature. However, at temperatures above 373°K, very few values of activity coefficient ($\gamma\pm$) are known in order to calculate the activity of the metal ion.

Lietzke and Stoughton[37] have shown rather conclusively that activity coefficients can be correlated by various Debye-Hückel expressions up to 523°K as easily as they are at room temperature. This method was further developed by Cobble[38] to predict solubilities of salts in water up to 523°K. These Debye-Hückel expressions show a decrease in activity coefficient with temperature, which can become very significant at higher concentrations.

Meissner, Kusik and Tester[39] have described a method, which utilizes vapour pressure measurement and the Gibbs-Duhem equation. However, this did not serve the purpose of

calculating the value of the activity coefficient of ferric chloride, due to the unavailability of data on its vapour pressure.

An attempt was therefore made to establish a relationship between the activity of ferric ion in equilibrium with hematite, and goethite. The solubilities of iron compounds at various elevated temperatures were estimated from a knowledge of the equilibria constants, which in turn were calculated from the standard free energy changes for each reaction according to equations:

$$\Delta G^{\circ}_{T} = -RT \ln K_{T}$$

$$\Delta G^{\circ}_{T} = \Delta G^{\circ}_{298} + \Delta C^{\circ}_{p}\Big]^{T}_{298} (T-298) - \Delta S^{\circ}_{298} (T-298) - T \Delta C^{\circ}_{p}\Big]^{T}_{298} \ln \frac{T}{298}$$

where

ΔG°_{298} = standard free energy of reaction at 298°K

ΔG°_{T} = standard free energy of reaction at T°K

ΔS°_{298} = standard entropy change of reaction at 298°K.

$\Delta C^{\circ}_{p}\Big]^{T}_{298}$ = the average heat capacity change for the reaction between 298° and T°K.

2.2.3 Hydrothermal Precipitation of Iron III Compounds

The degree to which leach solutions can be freed from ferric ion is dependent on the solubility of the precipitate. Feitknecht and Schindler[40] have critically reviewed the solubility relationships of iron III oxides and hydroxides at 298°K, and their findings are summarized on the basis of the following aging scheme:

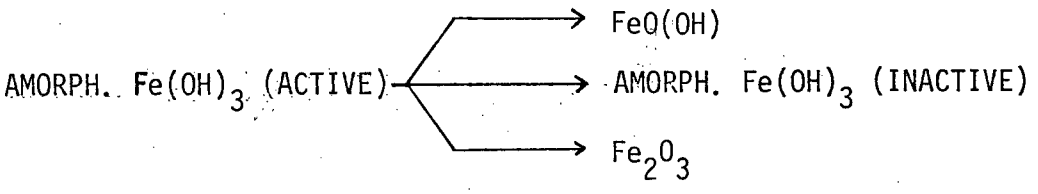

They proposed that freshly precipitated active amorphous hydroxide slowly converts to goethite. In addition, a solid transformation occurs resulting in a more stable amorphous hydroxide. Biedermann and Schindler[41] have shown that the complete transformation requires about 6 - 8 days, but less than one day at 373°K.[42] Goethite is stable at room termperature but dehydrates to hematite above about 403°K.[43] It is anticipated, that in leaching experiments at about 423°K, hematite is nucleated homogeneously by the hydrolysis reaction:

$$Fe^{3+} + \frac{3}{2} H_2O = \frac{1}{2} Fe_2O_3 + 3 H^+$$

Ferric hydroxide is unstable under such conditions of acidity and temperature, and will not be further considered.

2.2.4 Hematite-Goethite Relations in Acid Solutions

Tunell and Posnjak[44] cited an experiment in which goethite in 0.1MHCl solution was converted to hematite at 373°K. This decomposition required a few weeks. Gruner,[45] using goethite in distilled water, took about ninety days to effect this decomposition to hematite at temperatures of over 473°K. The qualitative effect of pH on the decomposition of goethite,[46] is that the decomposition temperature is near 373°K in acid solutions and above 423°K in alkaline solutions.

In light of the fact that the decomposition of goethite to hematite is kinetically a slow process, it is imperative that complete dissolution occurs to produce the ferric chloride intermediate for subsequent hydrolysis to hematite. Hydrolysis of ferric chloride[47] is known to occur at as low as 393°K.

2.2.5 The Effect of pH on the Solubility of Iron III Compounds Without Complexing

With knowledge of the working pH range during leaching experiments, and careful scrutiny of the iron E - pH diagrams,[51] only the Fe^{3+}_{aq} species was considered. For a relatively complete treatment of the iron-water relations, over 50 equilibria reactions are usually required to describe the solubility of a single compound. Furthermore, it should be pointed out that not only dissolved species for which free

energy values are available should be considered but, for example, $Fe(OH)_{3\,aq}$, or undissociated dissolved ferric hydroxide, because it may be an important contributor to iron solubility (J. Winchester, personal communication). Nevertheless, an attempt was made to show the relations of ferric ions, Fe^{3+}_{aq}, to the oxides and hydroxides of iron.

Table 2.2 shows values of the equilibrium constant obtained using equation 2.1, together with the associated pH, which were calculated using equation 2.4 and assuming that the activity of ferric ions in solution was unity.

It should be noted that lower pH values would be obtained for the hydrolysis reaction at higher concentrations, because Debye-Hückel expressions indicate a decrease in activity coefficient with temperature.[35]

2.2.6 Considering the Ferric Ion--Hematite Equilibrium

$$Fe^{3+}_{aq} + \frac{3}{2} H_2O_l = \frac{1}{2} Fe_2O_{3_C} + 3H^+_{aq}$$

The standard free energies for the hydrolysis of hematite at various temperatures (see Appendix A.3) were used to calculate the equilibrium constant via the relationship:

$$\text{Log } K = \frac{-\Delta G^\circ_T}{2.3\ RT} \qquad \ldots 2.1$$

Eliminating $Fe_2O_{3_C}$ and H_2O from the constant because their activity was assumed to be close to unity.

$$K = \frac{a_{H^+}^3}{a_{Fe^{3+}}} \qquad \ldots 2.2$$

and

$$\text{Log } K = 3 \text{ Log } a_{H^+} - \text{Log } a_{Fe^{3+}} \qquad \ldots 2.3$$

therefore

$$\text{Log } K = -3 \text{ pH} - \text{Log } a_{Fe^{3+}} \qquad \ldots 2.4$$

The log of the activity of Ferric ion in equilibrium with $Fe_2O_{3_C}$ is seen to be a linear function of pH, with a slope of minus 3. As a result, if a temperature and ferric ion activity are stipulated, then the pH is fixed.

At a leaching temperature of 423°K

$$\text{Log } [Fe^{3+}] = -4.8 - 3 \text{ pH} \qquad \ldots 2.5$$

The pH associated with various activities of ferric ion in equilibrium with hematite were calculated using equation 2.5. Activity values higher than 10^{-1} fall in such a high concentration range that a marked departure from molalities can be expected.

Table 2.2 Equilibrium Data for the Fe^{3+}—Fe_2O_3—H_2O System

Temperature °K	$\Delta G°_T$ Calories	Log K	PH
298	-2550	1.87	-0.62
333	-4774	3.13	-1.04
373	-6621	3.88	-1.29
423	-9295	4.80	-1.60
473	-11880	5.49	-1.83

2.2.7 Considering the Ferric Ion—Goethite Equilibrium

$$Fe^{3+} + 2H_2O = FeOOH + 3H^+$$

The free energy and pH values shown in Tables 2.4 and 2.5 were obtained in the similar manner described in section 2.2.6, and making the same assumption. At a leaching temperature of 423°K.

$$\text{Log } [Fe^{3+}] = 4.44 - 3pH$$

2.2.8 Considering the Ferric Ion—Ferric Hydroxide Equilibrium

$$Fe^{3+} + 3H_2O = Fe(OH)_3 + 3H^+$$

At a leaching temperature of 423°K

$$\text{Log } [Fe^{3+}] = -0.13 - 3pH$$

In constructing a pseudo phase diagram for the $Fe^{3+}—Fe_2O_3—H_2O$ system, the following expression is utilized to calculate the equilibrium pH at various temperatures and activities:

$$pH = \frac{1}{3}\left[-\log K - \log a_{Fe^{3+}}\right]$$

The same expression was utilized to calculate the equilibrium pH at various temperatures and activities for the $Fe^{3+}—FeOOH—H_2O$ metastable system.

Table 2.3 The pH Corresponding to Various Activities of Ferric Ion in Equilibrium with Hematite

Log $[Fe^{3+}]$	pH
0	-1.60
-1	-1.27
-2	-0.93
-3	-0.60
-4	-0.27
-5	-0.07

Table 2.4 Equilibrium Data for the Fe^{3+}—FeOOH—H_2O Metastable System.

Temperature °K	$\Delta G°_T$ Calories	Log K	pH
298	-2500	1.83	-0.61
333	-4250	2.79	-0.93
373	-6185	3.62	-1.21
423	-8598	4.44	-1.48
473	-10859	5.02	-1.67

Table 2.5 The pH Corresponding to Various Activities of Ferric Ion in Equilibrium with Goethite

Log $[Fe^{3+}]$	pH
0	-1.48
-1	-1.15
-2	-0.81
-3	-0.48
-4	-0.15
-5	-0.19

Table 2.6 Equilibrium Data for the Fe^{3+}—$Fe(OH)_3$—H_2O Metastable System

Temperature °K	$\Delta G°_T$ Calories	Log K	pH
298	4700	-3.45	1.15
333	3176	-2.08	0.69
373	1585	-0.93	0.31
423	-250	0.13	-0.04
473	-1826	0.84	-0.28

Table 2.7 The pH Corresponding to Various Activities of Ferric Ions in Equilibrium with Ferric Hydroxide

Log $[Fe^{3+}]$	pH
0	-0.04
-1	0.29
-2	0.62
-3	0.96
-4	1.29
-5	1.62

Table 2.8 Theoretical Equilibrium pH at Various Temperatures and Activities for the Fe^{3+}—Fe_2O_3—H_2O System

Temperature °K	Log K	Activity of Ferric Ions			
		1M	0.5M	0.2M	0.1M
		pH	pH	pH	pH
298	1.87	-0.62	0.52	-0.39	-0.26
333	3.13	-1.04	-0.94	-0.81	-0.71
373	3.88	-1.29	-1.19	-1.06	-0.96
423	4.80	-1.60	-1.49	-1.37	-1.27
473	5.49	-1.83	-1.73	-1.59	-1.49

Table 2.9 Theoretical Equilibrium pH at Various Temperatures and Activities for the Fe^{3+}—FeOOH—H_2O Metastable System

Temperature °K	Log K	Activity of Ferric Ions			
		1M	0.5M	0.2M	0.1M
		pH	pH	pH	pH
298	1.83	-0.61	-0.51	-0.38	-0.28
333	2.79	-0.93	-0.83	-0.70	-0.60
373	3.62	-1.21	-1.11	-0.97	-0.87
423	4.44	-1.48	-1.38	-1.25	-1.15
473	5.02	-1.67	-1.57	-1.44	-1.34

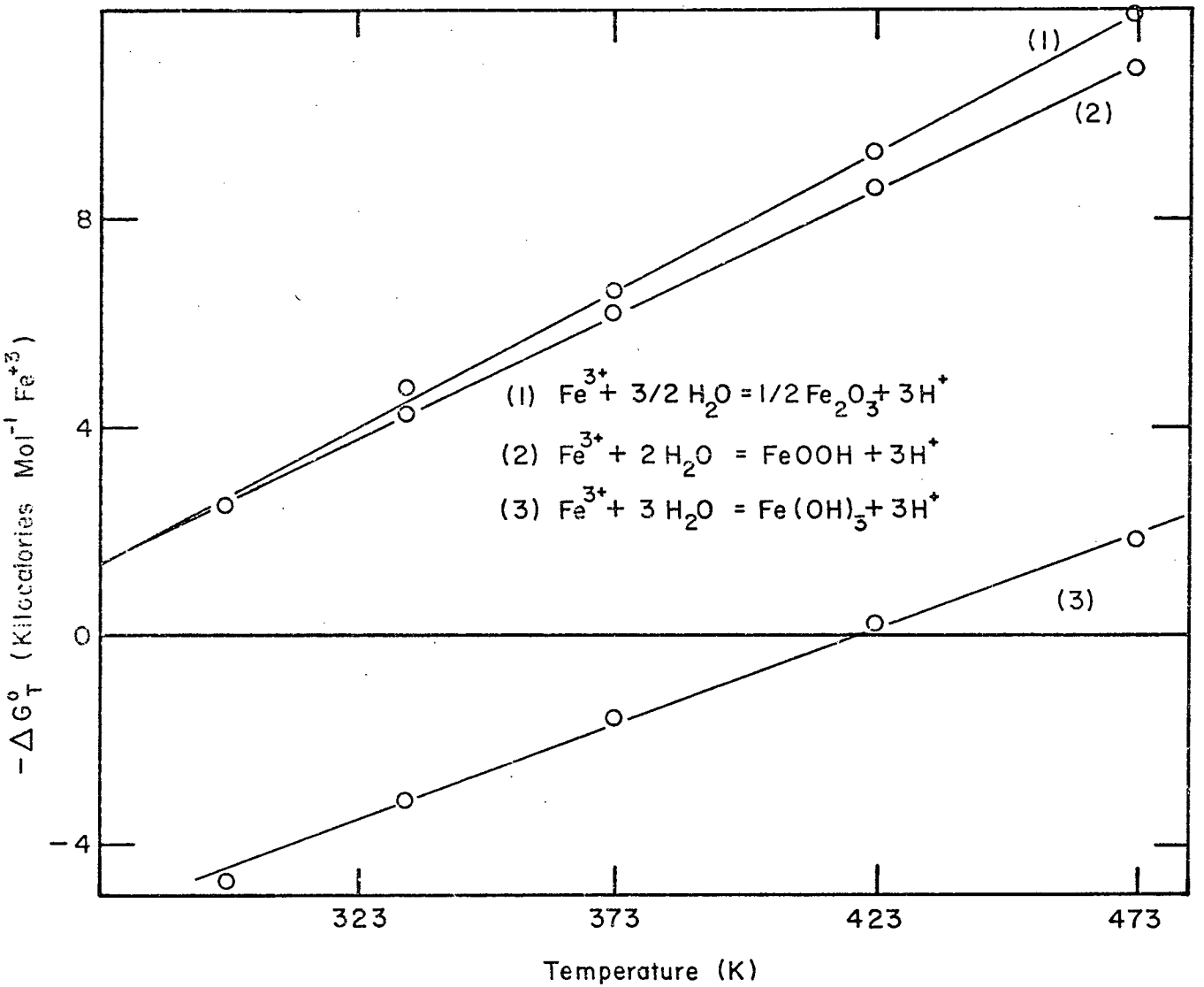

Figure 2.3 Free energy versus temperature for iron (III) hydrolisis reactions

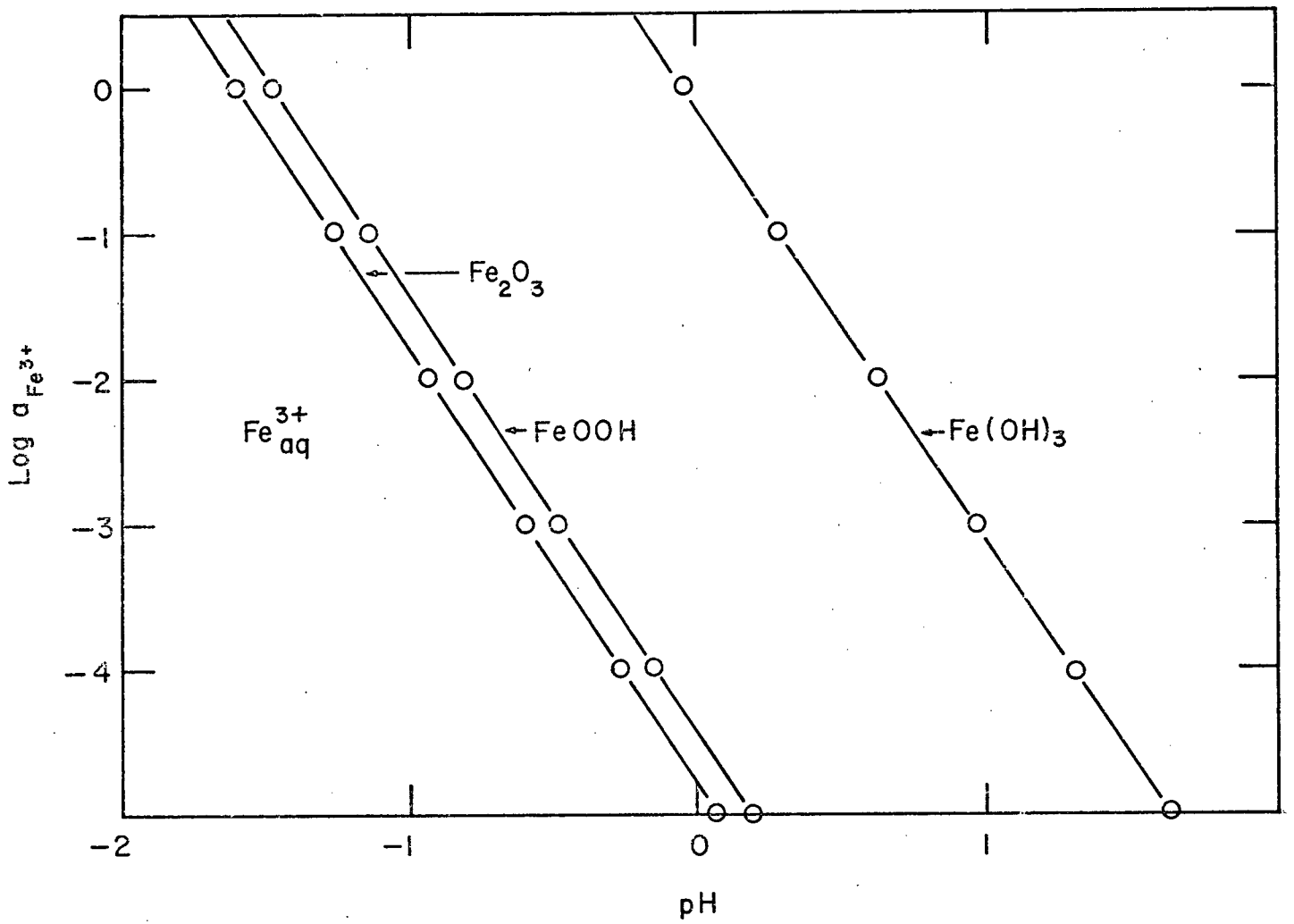

Figure 2.4 Influcence of pH on the solubility of iron (III) hydroxides and oxide at 423°K.

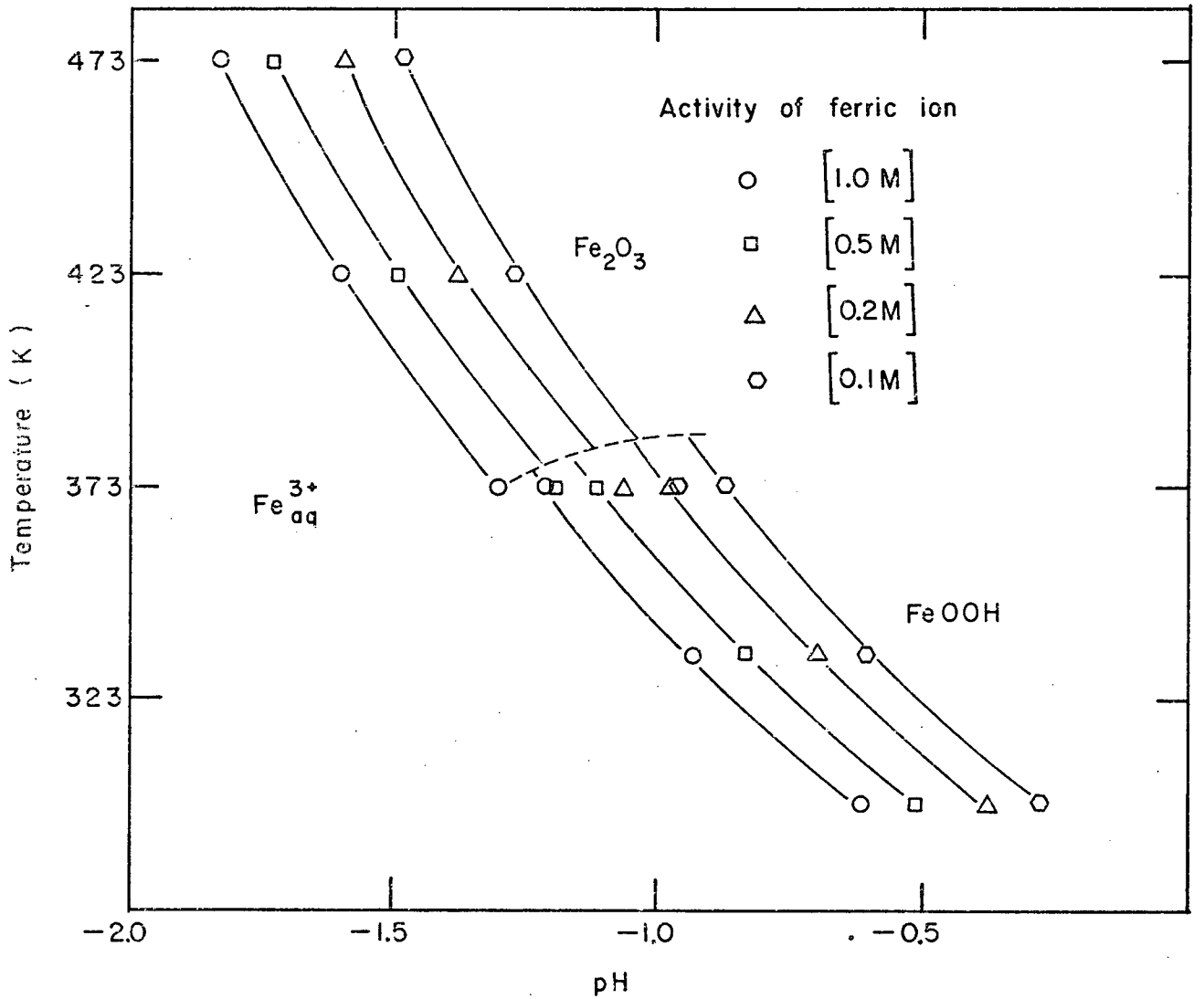

Figure 2.5 Temperature versus pH diagram for the Fe^{3+}— Fe_2O_3—H_2O system.

2.3 Thermodynamic Considerations Underlying the Hydrothermal Treatment of Nickel Laterite With Ferric Chloride

It has been shown[43] that the direct conversion of goethite to hematite is a relatively slow reaction. This can be thermodynamically explained by considering the free energy versus temperature relationship for hydrolysis reactions (see Figure 2.3).

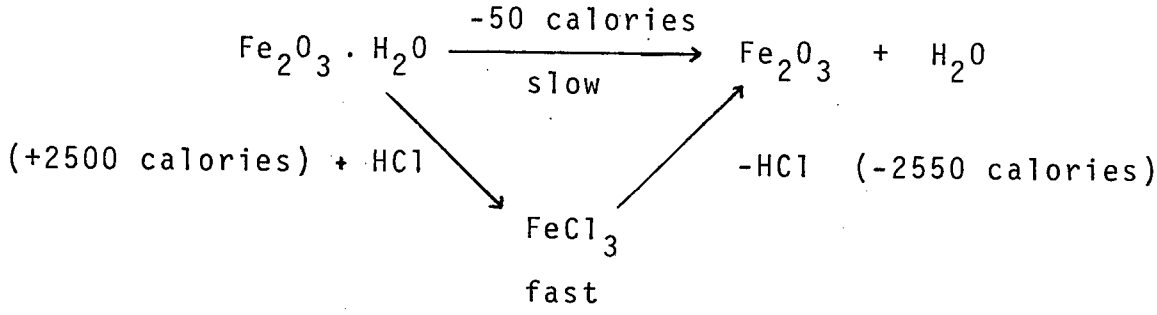

At 298°K, the conversion of goethite to hematite proceeds with a reduction of free energy of only approximately -50 calories.

Figure 2.3 also illustrates that the hydrolysis of hematite and goethite have similar thermodynamic driving forces, which increase with temperature. The hydrolysis of ferric hydroxide appears to be thermodynamically favored under standard conditions. Its presence however, is not expected under experimental conditions because of slow kinetics. Generally, the extent of hydrolysis[36] is enhanced by an increase in temperature and a decrease in the free acid level of the hydrolyzed liquor.

The overall conclusion therefore, is that the hydrolysis of hematite has the largest thermodynamic driving force, and this provides a possibility for a fast conversion of goethite to hematite under conditions where goethite can dissolve rapidly.

2.3.1 The Effect of Chloride Complexing

Due to the complexing power of chloride ion for ferric ions, the effect on ferric ion solubility should also be considered. Each complex predominates under different conditions of pH and ferric ion activity, and its effect on solubility can be estimated from equilibrium considerations.

Figure 2.4 illustrates the influence of pH on the solubility of hematite, goethite and ferric hydroxide. It should however be pointed out that these data are in terms of the ferric ion activity; the ferric ion activity is dependent on the degree to which it is complexed by chloride ions as well as by departures from ideality in strong solutions.

2.3.2 Temperature/pH Consideration

The pseudo-phase diagram of Figure 2.5 cannot serve to indicate the temperature of transformation of goethite to hematite. This must be done experimentally, by identification of the compounds precipitated at various

temperatures and pH.

Furthermore, the curves were obtained by assuming constant values of ferric ion activity with increased temperature. In fact, one can only assume the concentration remains constant, because the activity coefficient decreases with temperature. As a result, lower values of pH were calculated using the equation:

$$2xpH = \frac{\Delta G^{\circ}}{4.575T} - 2 \text{ Log } [M^{X+}]^{*}$$

instead of:

$$2xpH = \frac{\Delta G^{\circ}}{4.575T} - 2 \text{ Log } m_{M^{X+}} - 2 \text{ Log } \gamma_{M^{X+}}$$

While the pseudo-phase diagram may serve as a guide in describing the temperature-pH relationship, it is inaccurate, due to the unavailability of data on the activity coefficient as a function of temperature.

* Concentration (M)

Chapter 3

EXPERIMENTAL

3.1 Mineralogical Investigation

3.1.1 ENERGY DISPERSIVE X-ray ANALYSIS VIA SEM

The scanning electron microscope was utilized in determining the nature of a wide variety of particles found in the mineral sample supplied by Sherritt Gordon Mines Limited/Sherritt Research Centre, Fort Saskatchewan. Three discrete types of particles were identified.

1) Quartz or Silicate
   (Pale-yellow particles, which were relatively the largest observed.)

2) Chromite
   (Black or dark-brown particles, which were magnetically separated and smaller in size than those of quartz.)

3) Goethite
   (Redish-brown particles of very fine size, which possessed the highest nickel content.)

3.1.2 X-ray Diffraction Analysis

X-ray diffraction patterns of the ore sample, precipitated hematite and magnetic particles were obtained. The 2θ and relative intensity values were compared with those of the respective minerals, as given in the ASTM card. These values are reported in Tables B.1, B.2 and B.3 of Appendix B.

The ore sample was found to be composed mainly of goethite, which was poorly crystalline. There was no indication of a discreet nickel mineral such as garnierite. The presence of an appreciable amount of hematite was detected.

In each case, the relative intensities showed some variation. There was excellent agreement on the 2θ values of the peaks for hematite and chromite but not for goethite.

3.2 Quantitative Chemical Analysis

Several samples of nickel laterite were digested utilizing two standard methods of dissolution:

1) Hydrochloric/Nitric acid solution in the ratio 3:1

2) Perchloric acid dissolution after removal of organic matter with nitric acid.

Determinations were conducted by atomic absorption

spectrometry. The results obtained by the above methods were compared with those obtained from general testing laboratories.

Total Analysis of the ore is shown in Table 3.1.

3.3 Apparatus Design

An all titanium autoclave of 100 mls capacity was utilized. It was placed in a horizontally shaken heating jacket, which was connected to a thermistor temperature controller and voltage regulator. A potentiometer with a thermocouple was also employed to occasionally monitor the temperature. The main features of the apparatus are shown in Figure 3.2.

3.4 Pressure Leaching Experiments

3.4.1 Experimental Procedure

The experimental procedure consisted of the following steps:

1) The powdered sample (usually 16 gms) was added to 40 mls of solution.

2) A pressure of 4.1×10^6 Newton metre^{-2} nitrogen was employed to minimize vapour transport into tubing connections and valves.

3) The thermistor was set at the required temperature.

Table 3.1 Chemical Analysis of the Nickeliferous Laterite[1]

Element	Percentage wt. Obtained	Percentage wt. Obtained (General Testing Lab)
Fe	44.5[2]	44.60
Ni	1.25[3]	1.24
Co	0.15	0.14
Cr	2.24	2.28
Mn	1.08	1.08
Al	4.70	4.66
Mg	2.30	2.32
Ca	-	0.12
Si	-	2.72
LOI	9.68	9.68

[1]Source: Marinduque Nickle Mines, Philippines

[2]Supplier suggested 43.9

[3]Supplier suggested 1.27

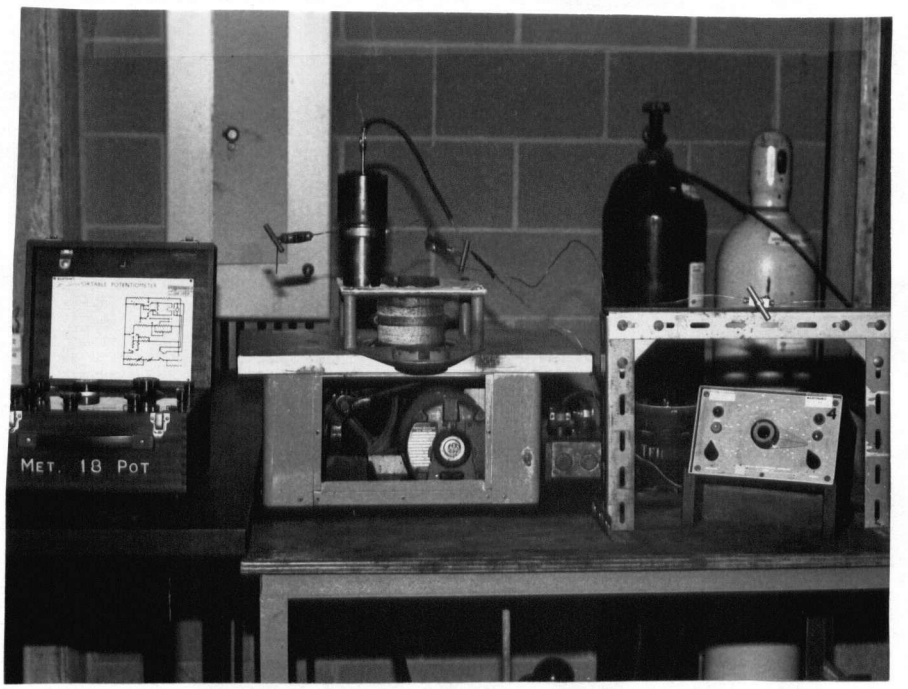

Figure 3.1 The leaching apparatus, showing from (L to R): the potentiometer, the titanium autoclave mounted on a shaking device, voltage regulator and the thermister controller.

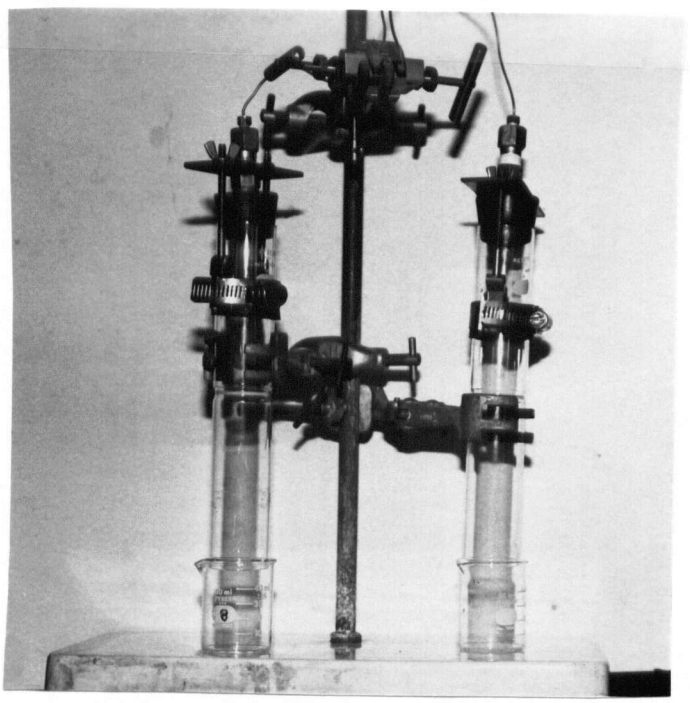

Figure 3.2 The pressure filter device.

4) Shaking was started with a constant heating rate corresponding to the maximum variac setting.

5) Ten degrees below the required temperature, the variac setting was adjusted to that corresponding to the required calibrated temperature.

6) The autoclave was quenched in a pail of water exactly one hour after having reached the desired leaching temperature.

3.4.2 Liquid/Solid Separation

Figure 3.1 shows the pressure filtration device, which was employed to speed up filtration, and at the same time prevent any evaporation of the filtrate. Although filtration was much faster with a buchner funnel and filter pulp, there were two disadvantages. Firstly, recovery of the iron residue was difficult when mixed with the pulp. Secondly, the hot filtrate evaporated to a certain extent due to the low pressure on the vacuum side of the filtering medium.

In order to reduce the contact time between the iron residue and the acidic filtrate, a laboratory centrifuge was employed. After about 5 minutes of centrifuging, the solution was decanted and the solids immediately swamped with water.

3.5 Analytical Methods

3.5.1 Atomic Absorption Analysis

Samples of filtrate were pipetted and diluted to the appropriate concentration for accurate measurement of their contents by atomic absorption spectrometry. Samples of the corresponding residues were digested and analyzed after thorough washing. A mass-balance technique was adopted as a means of checking the accuracy of the determinations.

Nickel, cobalt, iron, manganese, magnesium, aluminium and chromium were determined on a Perkin-Elmer 306 atomic absorption instrument. For all analyses, standards were first made up to approximate compositions of the unknown filtrate solutions. It was hoped that this procedure would compensate for the flame matrix effects of the filtrate solutions.

Flexibility in sample dilution was made possible by rotating the atomic absorption burner head, thereby changing the flame path length through which the beam was passed. Using this procedure, the linear portion of each element's absorption versus concentration curve was increased by approximately 20 times. (That is, by having the burner normal to the lamp beam line rather than co-linear with it.) Fewer sample dilutions were required by employing this technique.

3.5.2 Determination of "Free Acid"

The pH at which the precipitation of cations in chloride solutions occur were first determined, by adding metal chloride solutions to the same aliquot portion of standard hydrochloric acid, and titrating with sodium hydroxide.

An autotitrator in the inflection mode of operation produced the curves shown in Figure 3.3. These curves served to indicate the relationship between the pH value at which hydrolysis occurs and volume of titrant.

A symmetric titration curve is produced when the indicator electrode is reversible, and when there are an equal number of titrant reagent and reactant species in the equivalence equation. In a simple acid-base pH titration, the pH titration curve for equation (3.1) is symmetric.

$$H^+ + OH^- = H_2O \quad \ldots(3.1)$$

$$Fe^{3+} + 3OH^- = Fe(OH)_3 \quad \ldots(3.2)$$

A titration error can however, be generated if the solution contains a species, which chemically interferes with the titrant or reactant and in so doing, distorts the symmetry of the titration curve (equation (3.2)). This error is greatest when the equilibrium constant for the reaction between the reactant (or the titrant) and an interfering species is

Table 3.2 pH Values of Hydroxides in Equilibrium with Their Metal Ions

Hydroxides	pH	Published Data	
	0.5M[M^{n+}]	1M[M^{n+}]	.001 M[M^{n+}]
$Fe(OH)_3$	2.1	1.61	2.61
$Al(OH)_3$	3.5	3.22	4.22
$Cr(OH)_3$	4.5	3.93	4.93
$Ni(OH)_2$	7.2	6.09	7.49
$Mn(OH)_2$	8.4	7.65	9.15
$Mg(OH)_3$	9.5	8.48	9.98
$Fe(OH)_2$	6.5	6.65	8.15

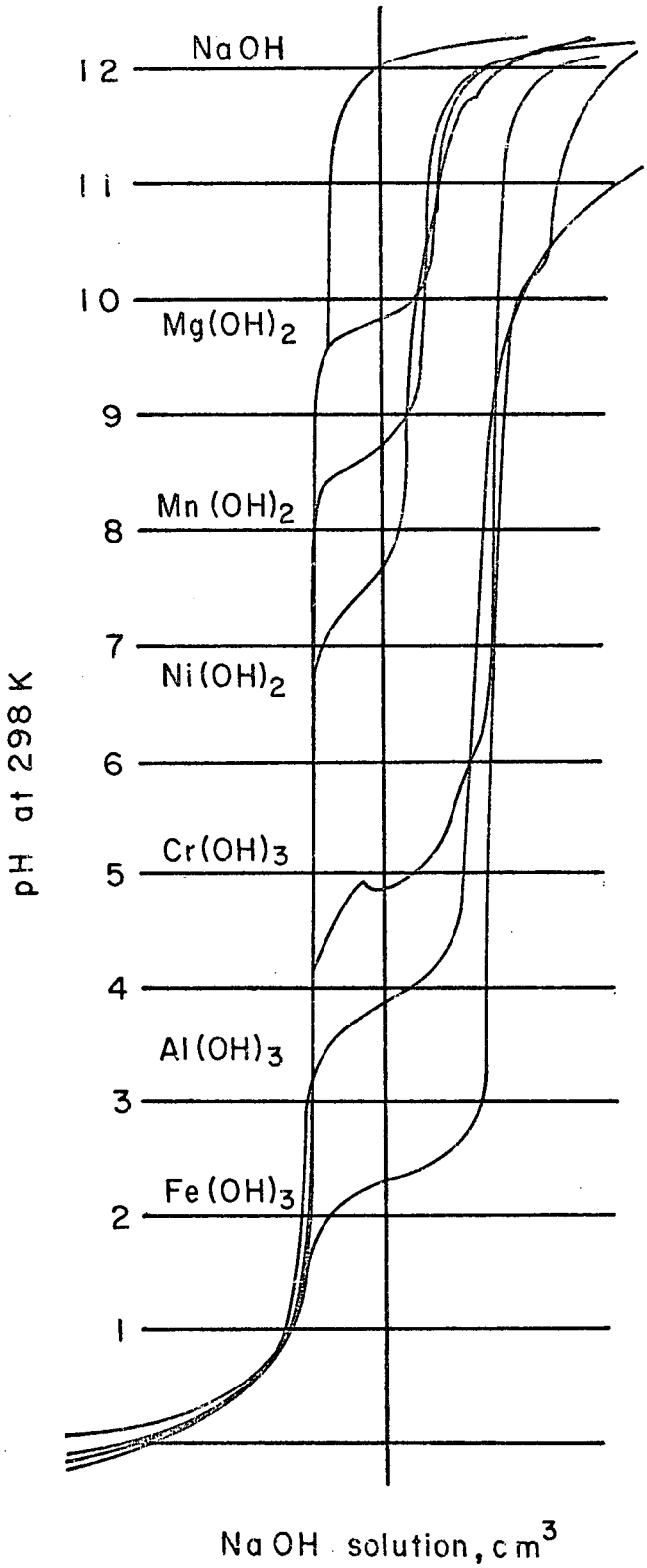

Figure 3.3 pH titration curves of metal chlorides in hydrochloric acid versus sodium hydroxide.

close to that of the reaction between the titrant and the reactant. If the interference reaction is with the titrant a second end point may be seen. In acid-base ph titrations, an acid strength difference of six orders of magnitude ($\Delta pK = 6$) is required for the clean separation of two end points (Basset et al., 1978). However, the magnitude of this type of titration error depends heavily on the relative quantities of the species involved.

Table 3.2 shows the pH at which the hydrolysis of several chlorides occur. It also shows the variation in pH values with the relative quantities of species involved in the $M^{n+}—M(OH)_n$ equilibrium. Figure 3.3 illustrates how close the pH value corresponding to neutralization of the "Free Acid" is to that for the hydrolysis of ferric ions in solution. For this reason, direct titration of the filtrate with 2N NaOH solution, with the auto-titrator in the derivative mode, resulted in very broad peaks. In most cases, the points of inflection on pH titration curves were also unsatisfactory.

An alternative method was therefore devised in determining the "Free Acid" concentration of the filtrate. In this procedure, an accurately measured volume of standard 2N hydrochloric acid was added to an aliquot of the filtrate. Any extra volume of 2N sodium hydroxide, beyond that which was required to neutralize the acid, was obtained by finding the difference.

Chapter 4

RESULTS

4.1 The Leaching of Nickeliferous Laterite in Aqueous Ferric Chloride

All leaching tests were performed in the 100 ml capacity titanium autoclave, the temperature of which was controlled to ± 2°K. The extractions of nickel, cobalt, manganese and chromium were determined as a function of:

1) Temperature ranging from 373°K to 473°K.
2) Concentration of ferric chloride ranging from 0.5M to 4.0M.
3) Pulp density ranging from 100 g/l to 400 g/l.

4.1.1 Effect of Temperature

Using 1 and 2 molar ferric chloride solutions with a constant 1 hour reaction time, the effect of reaction temperature is shown in Figure 4.1. In general, metal extraction increased with increasing temperature (see leaching results of Table 4.1). At 423°K, nickel extraction was over 90 percent, provided the concentration of ferric chloride was greater than

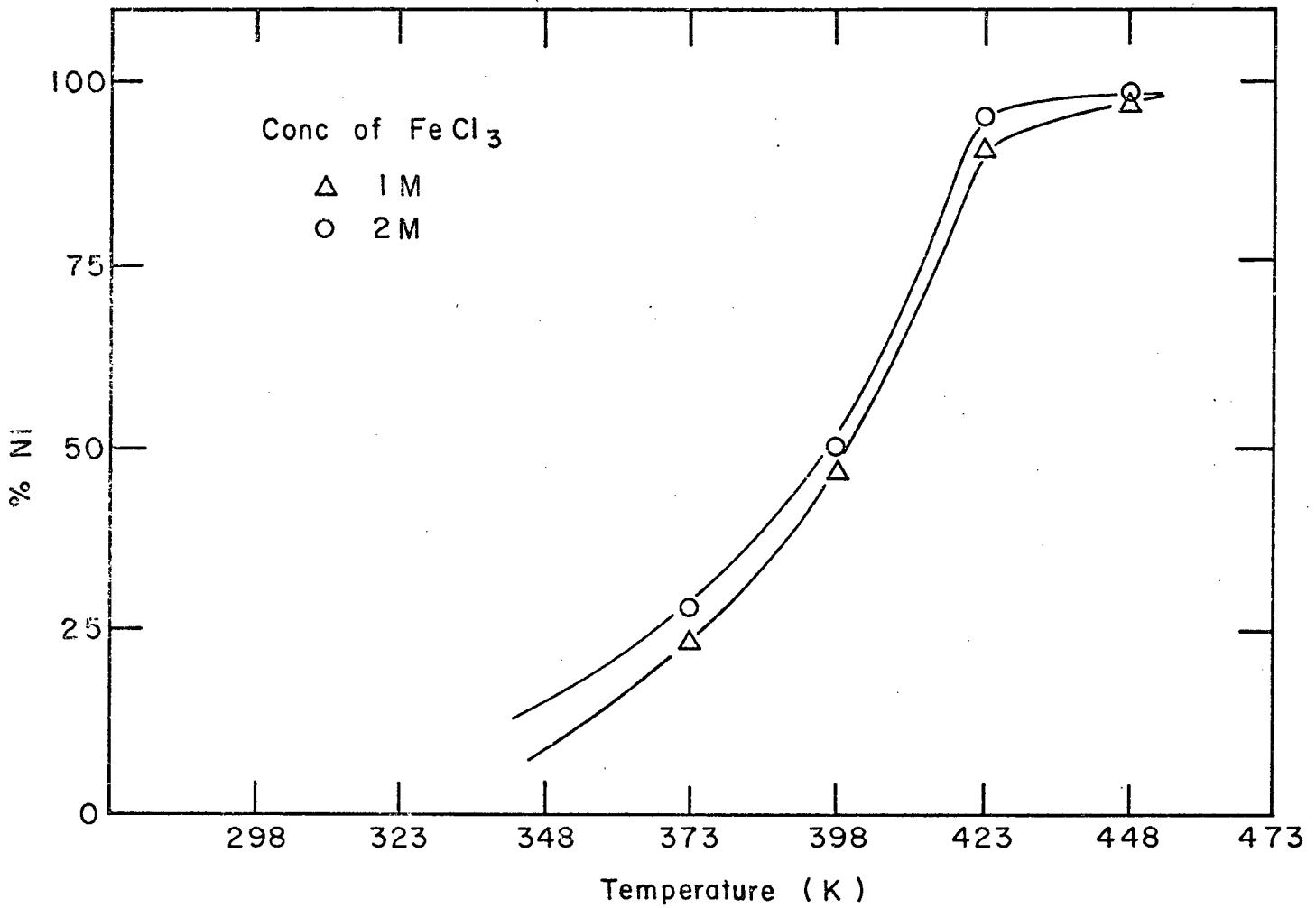

Figure 4.1 Effect of temperature on nickel extraction from nickeliferous laterite

Table 4.1 Metal Extraction From Nickeliferous Laterite with Aqueous Ferric Chloride

Solution Type $FeCl_3$(M)	Temp. °K	Pulp Density g/l	Metal Conc. in Filtrate gpl				% Ni Extraction
			Ni	Co	Cr	Mn	
0.5	448	100	1.2	0.15	0.16	1.0	96
0.5	448	200	2.1	0.30	0.19	1.9	84
1.0	373	200	0.6	1.10	0.14	0.7	24
1.0	398	200	1.2	0.20	0.21	1.3	48
1.0	423	200	2.4	0.30	0.38	2.0	96
1.0	448	200	2.5	0.30	0.21	2.2	98
1.0	448	300	3.4	0.45	0.20	3.0	91
2.0	373	200	0.7	0.10	0.19	0.8	28
2.0	398	200	1.2	0.23	0.28	1.5	50
2.0	423	200	2.4	0.30	0.50	2.1	96
2.0	448	200	2.5	0.30	0.40	2.2	98
2.0	448	300	3.6	0.45	0.28	3.1	96
1.0	373	100	0.31				25
1.0	423	100	1.24				99
1.0	473	100	1.24				99
1.0	523	100	1.24				99
1.0	423	400	4.3				88
2.0	423	400	4.9	0.60	0.45	4.0	96

1M. The concentration of chromium in the filtrate increased with increasing temperature up to around 423°K but decreased at higher temperatures. This behaviour was suspected to be due to the precipitation of a ferric-chromium complex.

4.1.2 Effect of Concentration

Figures 4.1 and 4.2 show the effect of ferric chloride concentration on nickel extraction. At low temperatures, 348°K, the percentage metal extraction was more dependent on ferric chloride concentration whereas leaching at higher temperatures resulted in almost the same percentage extraction irrespective of concentration.

4.1.3 Effect of Pulp Density

The pulp density of the leach did not appear to have any significant effect on metal extraction, provided enough reaction time was allowed and sufficient chloride ions were available. With pulp densitites of 100 g/l, 200 g/l and 400 g/l, nickel extraction at 423°K, with 1M ferric chloride solution was 98 percent, 96 percent and 90 percent respectively. Figure 4.3 illustrates this effect in the form of a curve, which is nearly horizontal. Figure 4.2 shows low values of percentage nickel extraction, which were obtained at pulp densities of 300 g/l and 400 g/l. Such low percentages were

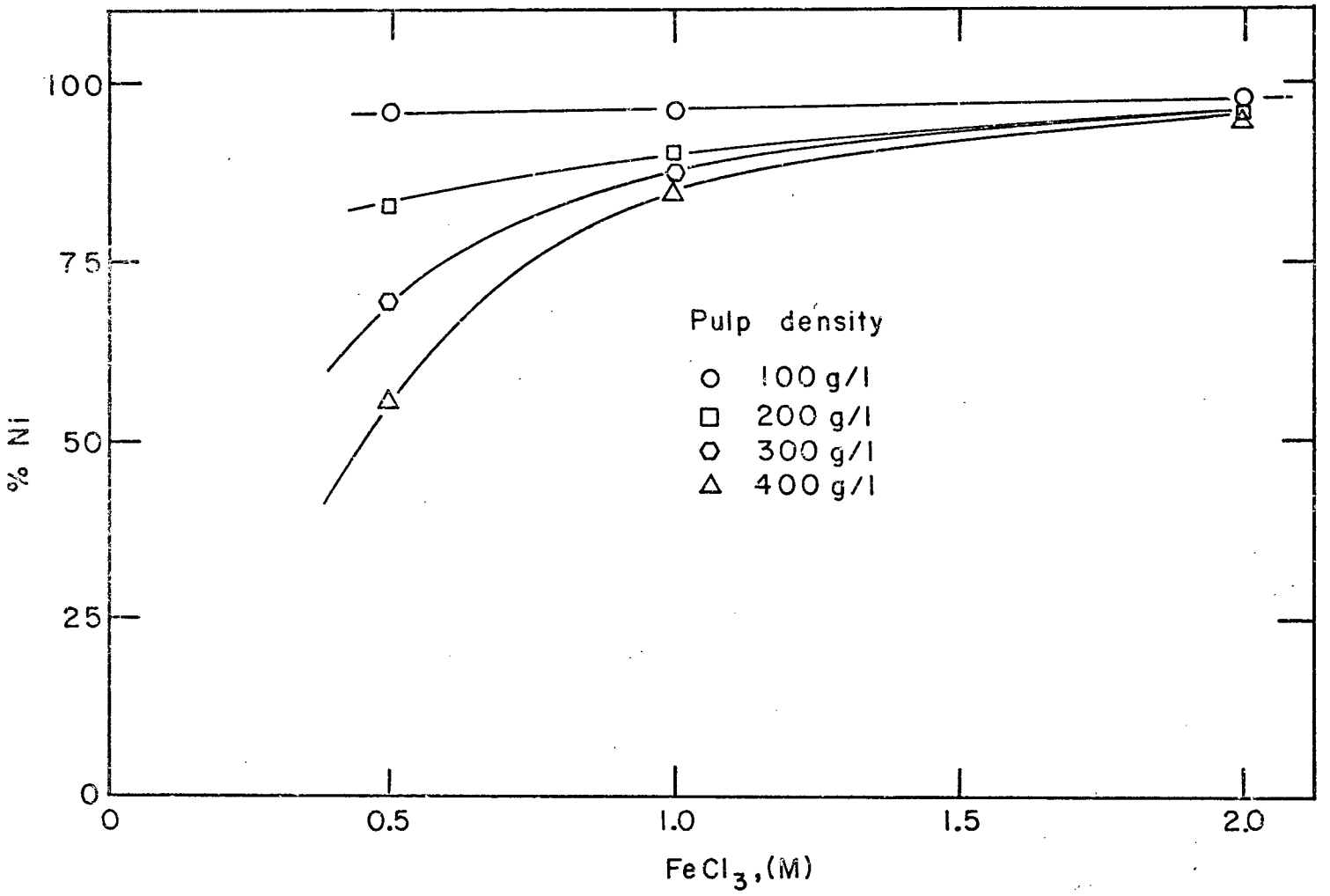

Figure 4.2 Effect of $FeCL_3$ concentration on nickel extraction at 448°K.

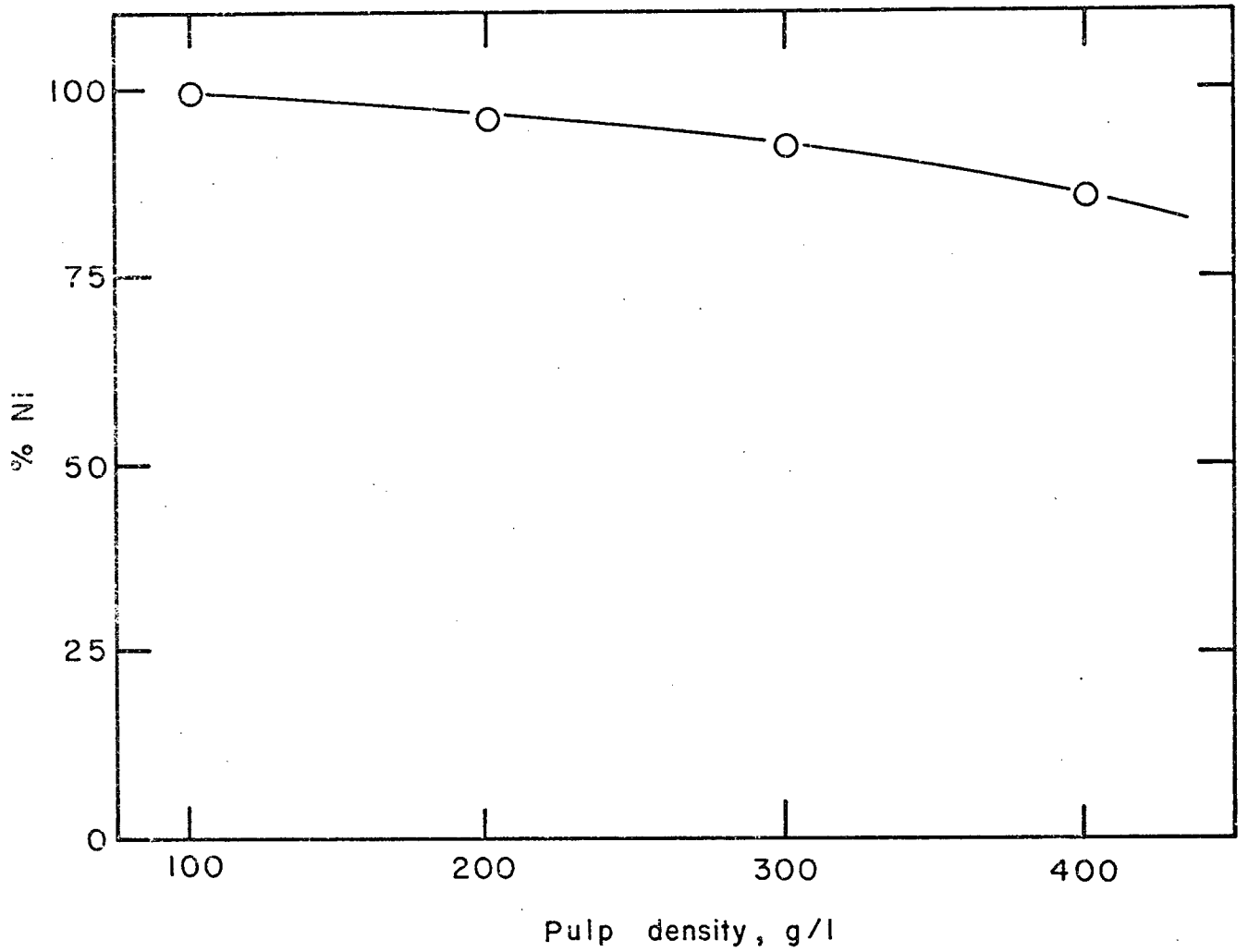

Figure 4.3 Effect of pulp density on nickel extraction with 1M $FeCl_3$ at 423°K.

to be expected because of the low concentration of ferric chloride solution employed and the subsequent unavailability of sufficient chloride ions to react with metal values contained in the ore.

4.2 The Leaching of Nickeliferous Laterite in Ferric Chloride/Hydrochloric Acid Solutions

It was postulated that the presence of higher amounts of "free acid" would not only increase metal recovery at lower temperatures, but also reduce the consumption of ferric chloride - a more expensive reagent. Various acidified ferric chloride solutions were prepared from a stock solution of hydrochloric acid, and used as the lixiviant.

As shown in Figure 4.4. nickel extraction was more sensitive to ferric chloride concentration than to that of hydrochloric acid. In fact, it was apparent that the presence of acid slightly decreased nickel extraction and greatly increased the amount of iron leached into solution. The latter, however, occurred only when there was an excess of "free acid" over that which was required to react with all the metal consitituents of the laterite. It should be noted that maximum nickel extraction in the presence of "free acid" occurred only with a ferric chloride concentration greater than 1.5 M.

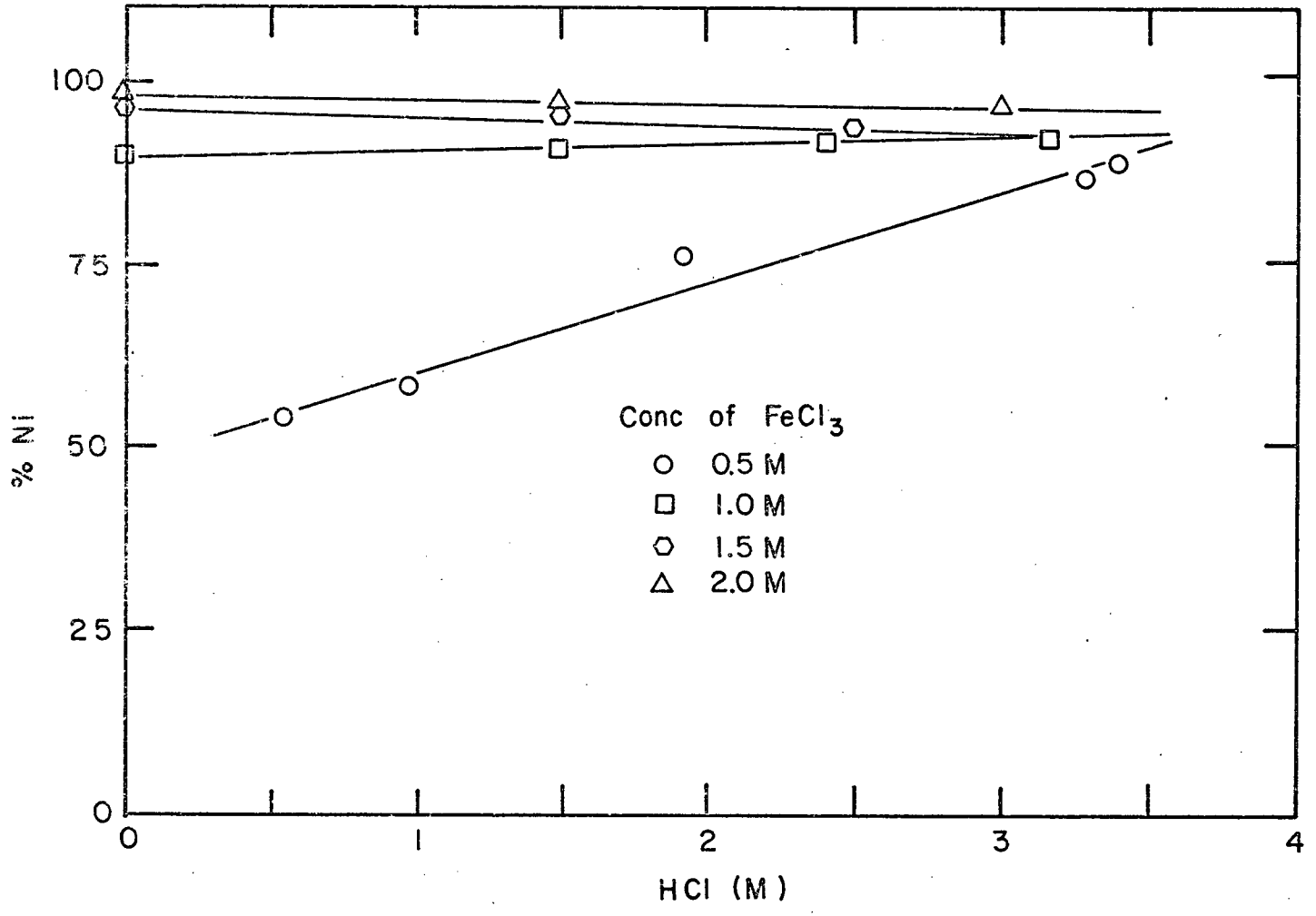

Figure 4.4 Effect of "Free Acid" concentration at several $FeCl_3$ concentrations on nickel extraction at 423°K and a pulp density of 400 g/l

Table 4.2 Leaching Results in the Presence of "Free Acid" at 423°K

Solution Type		Pulp Density	Ni Conc. in Filtrate	% Nickel	Fe Conc. in Lixiviant	Fe Conc. in Filtrate	"Free Acid" in	"Free Acid" Consumed
$FeCl_3$(M)	HCl(M)	g/l	gpl	Extraction	gpl	gpl	Filtrate	HCl(M)
0.24	2.00	200	2.1	82	13	23	0.17	1.83
0.45	1.93	200	2.2	88	25	33	0.17	1.76
0.86	1.79	200	2.3	90	48	53	0.11	1.68
1.57	1.50	200	2.4	96	88	88	0.05	1.45
0.24	2.00	400	3.0	60	13	6.3	0.09	1.91
0.45	0.55	400	2.7	54	26	0.2	0.08	0.47
0.45	0.98	400	2.9	58	25	1.2	0.09	0.89
0.45	1.93	400	3.8	76	25	14	0.09	1.84
0.58	3.28	400	4.3	86	33	44	0.09	3.19
1.57	1.50	400	4.7	94	88	62	0.05	1.45
0.47	3.39	400	4.4	88	26	38	0.09	3.30
0.86[1]	3.16	400	2.5	50	48	75	0.04	3.12
0.86	3.16	400	4.5	90	48	55	0.02	3.14
1.52	2.84	400	4.6	92	85	85	0.02	2.82
1.92[2]	3.00	400	4.2	84	107	110	0.09	2.91

[1] Leaching time 15 minutes.

[2] Leaching in a large autoclave (2 litres capacity) with very little agitation.

Table 4.2 shows the leaching results obtained using ferric chloride/hydrochloric acid solutions. Higher concentrations of iron in the filtrate as compared to the corresponding lixiviant were due to dissolution of precipitated hematite. The concentration of iron remained the same, whenever the acid concentration employed was equal to the theoretical amount, which is required to react with the metal constituents of the ore (as described in Section 4.4). The use of acid concentrations less than this theoretical value resulted in the hydrolysis of ferric chloride. The extent of hydrolysis depended on the concentration of acid used and was reflected in the decrease of iron concentration in the filtrate as compared to that in the lixiviant.

4.3 Leaching of Nickeliferous Laterite in the Presence of Ferrous Chloride

Ferrous chloride reagent was utilized in an effort to retard the rate of precipitation of hematite. It was envisaged that the particle size of the precipitate would increase, thereby speeding up filtration.

It was observed however, that the presence of ferrous chloride, to a greater extent than hydrochloric acid, inhibited the extraction of nickel. Table 4.3 shows the effect of ferrous chloride on nickel extraction.

Table 4.3 Leaching Results in the Presence of Ferrous Chloride at a Pulp Density of 400 g/l.

Solution Type	% Nickel Extraction	Fe Conc. in Lixiviant gpl	Fe Conc. in Filtrate gpl	Acid Consumed HCl(M)
1M $FeCl_2$	36	51	43	-
1M $FeCl_2$, 3M HCl	71	55	59	2.80
0.5M $FeCl_2$, 0.5M $FeCl_3$, 3M HCl	88	55	55	2.76
1M $FeCl_3$, 3M HCl	94	55	55	2.82
1M $FeCl_3$	90	55	12	-

4.4 Acid Consumption During a Batch Leach (423°K)

Table 4.4. shows the amount of acid consumed in reacting with each metal species present in the laterite, with the exception of iron. These values were calculated by using the concentration of each metal in the filtrate. The total value represented the quantity of acid to be replenished after each leaching cycle, providing there was no additional hydrolysis reaction to supply acid.

Table 4.4 Acid Consumption During a Batch Leach at 423°K with a Pulp Density of 400 g/l.

Metal	Metal Conc. in Filtrate gpl	Acid Consumption by Individual Metal gpl	Equivalent Acid Concentration HCl(M)
Co	0.6	0.74	0.02
Cr	0.5	1.05	0.03
Mn	4.1	5.58	0.15
Ni	5.0	6.21	0.17
Mg	8.0	24.00	0.66
Al	14.6	59.19	1.62
Total		96.77	2.65

The calculated value of 2.65M hydrochloric acid compare favorably with 2.82M, which was obtained using the auto-titration method. The slightly higher value of acid consumed was to be expected, taking into consideration further dissolution of finely precipitated hematite, during the period of time taken to dismantle the apparatus and filter the solids.

An attempt was therefore made to determine if in fact a portion of the "free acid" did become consumed in the dissolution of finely precipitated hematite after leaching.

A laboratory centrifuge was employed to reduce the period of time during which the solution was in contact with the iron residue. By reducing this period from 1 hour to 15 minutes, there was an increase in "free acid" concentration from about 0.05M to approximately 0.2M. This was however, still lower than the theoretical value of about 0.5M.

This was confirmed by determining the concentration of "free acid" produced by heating ferric chloride solutions alone, at temperatures of 423°K and 453°K. The acid results obtained due to hydrolysis were compared with those obtained after leaching with ferric chloride and acid / ferric chloride mixtures. In one experiment, the slurry obtained after leaching was allowed to stand for 13 hours, and the "free acid" concentration in the filtrate fell to a lower value. The concentration of iron increased slightly. The results obtained are shown in Table 4.5.

4.4.1 The Effect of Hydrolysis on Acid Consumption

Hydrolysis of ferric chloride[47] is known to begin at around 393°K, producing hematite and hydrochloric acid. Table 4.5 shows that at room temperature, the "free acid" concentration in ferric chloride solution was 0.06M. However, hydrolysis of this solution at temperatures, 423°K and 453°K resulted in "free acid" concentration of 0.38M and 0.50M

Table 4.5 Comparison of "Free Acid" Concentration in Filtrates with Acid Concentration Due to the Hydrolysis of Ferric Chloride

Solution Type $FeCl_3$	HCl	Temperature °K	Pulp Density g/l	Fe Conc. in Lixiviant gpl	Fe Conc. in Filtrate gpl	"Free Acid" in Lixiviant HCl(M)	"Free Acid" in Filtrate HCl(M)
2M	-	423	-	112	109	0.06	0.38
2M	-	453	-	112	106	0.06	0.50
2M	-	423	400	112	60	0.06	0.07
2M	-	453	400	112	58	0.06	0.03
2M,	3M HCl	423	400	110	113	3.00	0.02
2M,[1]	3M HCl	453	400	110	115	3.00	0.003

[1]Slurry from this run was allowed to stand for 13 hours.

respectively. This increase in acid concentration coincided with a decrease in iron concentration of the filtrate.

Leaching experiments were conducted at the same temperatures, employing the same concentration of ferric chloride. Lower values of iron concentration in the filtrate indicated that further hydrolysis occurred, in order to supply more acid necessary to react with metal values present in the ore. The "free acid" level in the filtrate approximated to that in the lixiviant.

In another leaching experiment, an excess of hydrochloric acid (over that which was required for complete metal extraction), was added to a lixiviant solution containing the same amount of ferric chloride used before. A slightly higher concentration of iron in the filtrate indicated some dissolution of the iron residue. Further dissolution was observed on leaving the leach slurry to stand for 13 hours.

It follows therefore, that dissolution of the ore gradually occurred, producing a ferric chloride intermediate, which was promptly hydrolysed to hematite. Once enough acid was present in the lixiviant, hydrolysis of ferric chloride contained in the latter was probably insignificant. It is not known at this stage, what proportion of the hematite precipitated from ferric chloride of the lixiviant or from dissolved laterite.

4.4.2 "Free Acid" Concentrations in Ferric Chloride Solutions

Several concentrations of ferric chloride solution were heated under the same conditions used for leaching experiments. The hematite collected was weighed and the filtrate analysed for iron and "free acid" concentration. Table 4.6 shows the percentage of iron precipitated from these solutions along with their acid concentrations. The extent to which hematite is precipitated from ferric chloride solutions, and the amount of "free acid" thereby being released are illustrated in Figure 4.5.

At ferric chloride concentrations greater than 1M, the quantity of acid liberated due to hydrolysis was more dependent on temperature than on concentration of the former. In one experiment, using a 1 molar ferric chloride solution, the concentration of hydrochloric acid determined was 0.39M at 423°K, as compared to 0.53M at 453°K.

4.5 The Determination of Leaching Equilibrium

Calculated amounts of nickel chloride hexahydrate were added to each batch of leach solution to give 20 gpl, 40 gpl and 60 gpl nickel respectively. Leaching experiments were conducted at 423°K and 448°K, and the iron residue obtained was carefully washed and analysed.

Table 4.6 Iron Precipitation From Ferric Chloride Solutions at 423°K.

Fe.Conc. in Solution gpl	Fe Conc. in Filtrate gpl	wt. of Fe Precipitated gms	Percentage Precipitation of Fe	"Free Acid" Conc. in Filtrate HCl(M)
27.2	19.8	7.4	27	0.51
54.4	47.5	7	13	0.50
109	105	4	3.7	0.39
110	104	6	5.4	0.53[1]
217	215	2	0.01	0.41[2]

[1] Determined at 453°K.

[2] Determined at 433°K.

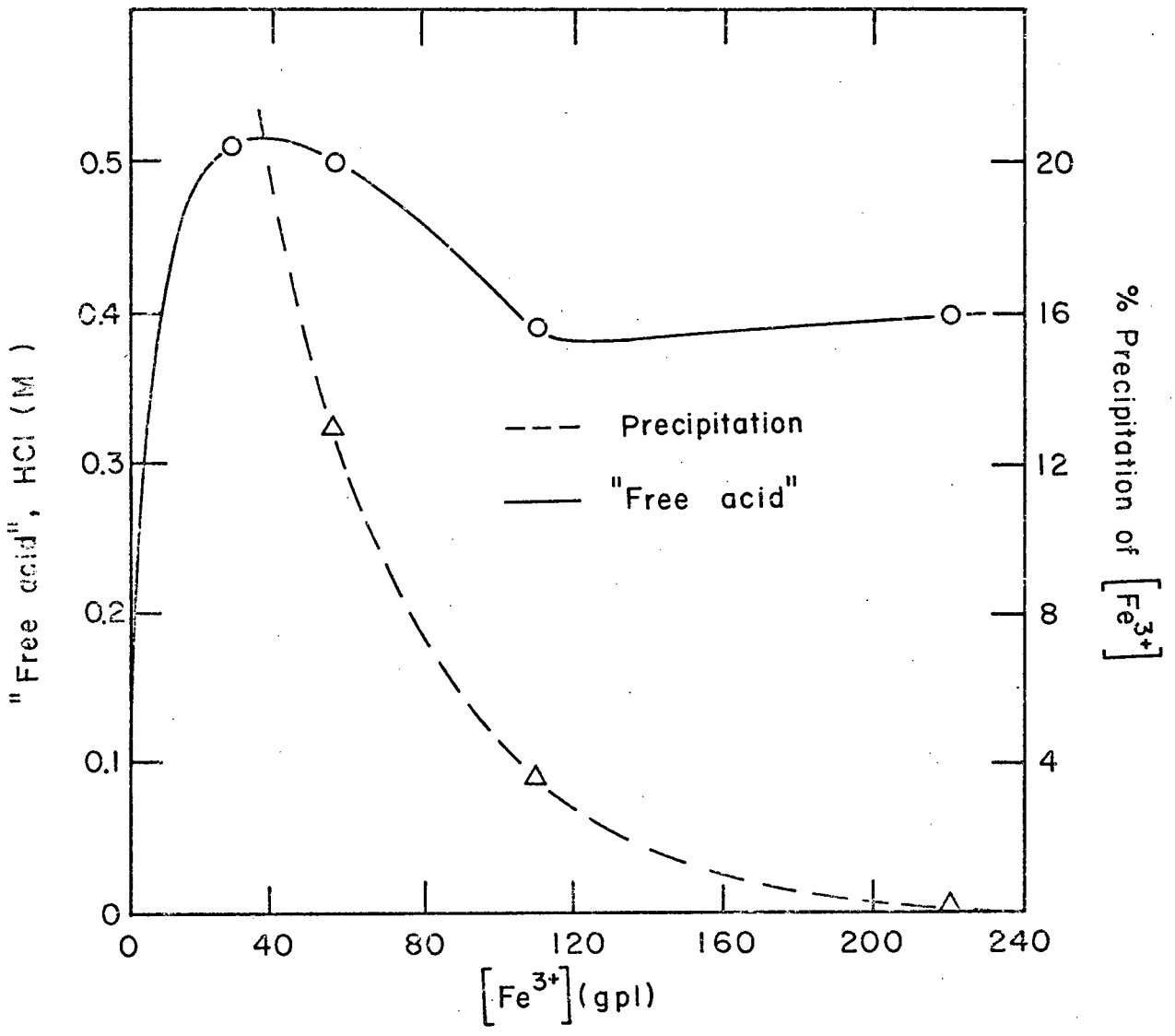

Figure 4.5 "Free Acid" concentration and percentage iron precipitation versus iron (III) concentration at 423°K.

Results shown in Table 4.7 indicate that at 423°K over 90 percent nickel can be extracted with 1M ferric chloride reagent, in the presence of up to 60 gpl nickel.

Table 4.7 Percentage Nickel Extraction from Nickeliferous Laterite in the Presence of High Concentrations of Nickel

Solution Type	Pulp Density gpl	Nickel Conc. in Filtrate gpl	Percentage Nickel Extraction
20 gpl Ni, 2M $FeCl_3$	200	22.5	98.4
40 gpl Ni, 2M $FeCl_3$	200	42.2	97.6
60 gpl Ni, 2M $FeCl_3$	200	62.5	95.2
60 gpl Ni, 1M $FeCl_3$	200	62.0	91.2

4.6 Simulation of a Continuous Leaching Circuit

A constant chloride ion activity was maintained by adding calculated amounts of 6N magnesium chloride, aluminium chloride, and ferric chloride to a constant volume of 9.6N hydrochloric acid. These chlorides were known to be the main constituents of the filtrate. The total volume of the lixiviant in each leaching cycle was the same, and the final acid concentration

Was 2.4N hydrochloric acid. A Similar run with only 6N ferric chloride solution was conducted and the results obtained are shown for comparison (see Table 4.8).

Figure 4.5 illustrates how a decrease in ferric chloride concentration, despite a constant acid concentration, resulted in a decrease in the percentage of nickel extracted. Cobalt and manganese showed similar extraction behaviours, whilst very little chromium was extracted. The extraction of aluminium and magnesium decreased gradually as a result of the decrease in ferric chloride concentration, and/or because of the common ion effect.

4.7 Morphology of the Iron Residue

4.7.1 Hematite from the Hydrolysis of Ferric Chloride

The Scanning Electron Microscope was employed to scrutinize particles obtained from each of the experiments described in Section 4.4.2. There was no detectable difference, in the nature, shape and size of the particles obtained at different temperatures - only in the quantity of precipitate (see Table 4.6).

There was however, an increase in particle size of the hematite precipitated from ferric chloride solutions ranging

Table 4.8 Percentage Metal Extraction in a Simulated Continuous Leaching Circuit

Lixiviant Composition		Metal Conc. in Lixiviant gpl	Fe Conc. in Filtrate gpl	Percentage Metal Extraction					
Solution Type	Volume (mls)			Ni	Co	Mn	Cr	Al	Mg
			Stage 1						
6N $FeCl_3$	40	110	60	98	91	91	20	78	76
			Stage 2						
9.6N HCl	10								
6N $FeCl_3$	30	82.5	75	91	90	91	20	76	75
6N $AlCl_3$	-								
6N $MgCl_2$	-								
			Stage 3						
9.6N HCl	10								
6N $FeCl_3$	22.5	62	58	85	89	90	20	74	74
6N $AlCl_3$	5	6							
6N $MgCl_2$	2.5	5							
			Stage 4						
9.6N HCl	10								
6N $FeCl_3$	15	41	60	65	85	88	20	59	49
6N $AlCl_3$	10	12							
6N $MgCl_2$	5	10							
			Stage 5						
9.6N HCl	10								
6N $FeCl_3$	7.5	21	42	56	75	77	20	48	25
6N $AlCl_3$	15	18							
6N $MgCl_2$	7.5	15							
			Stage 6						
9.6N HCl	10								
6N $FeCl_3$	-	-	26	50	48	62	20	16	15
6N $AlCl_3$	20	24							
6N $MgCl_2$	10	19							

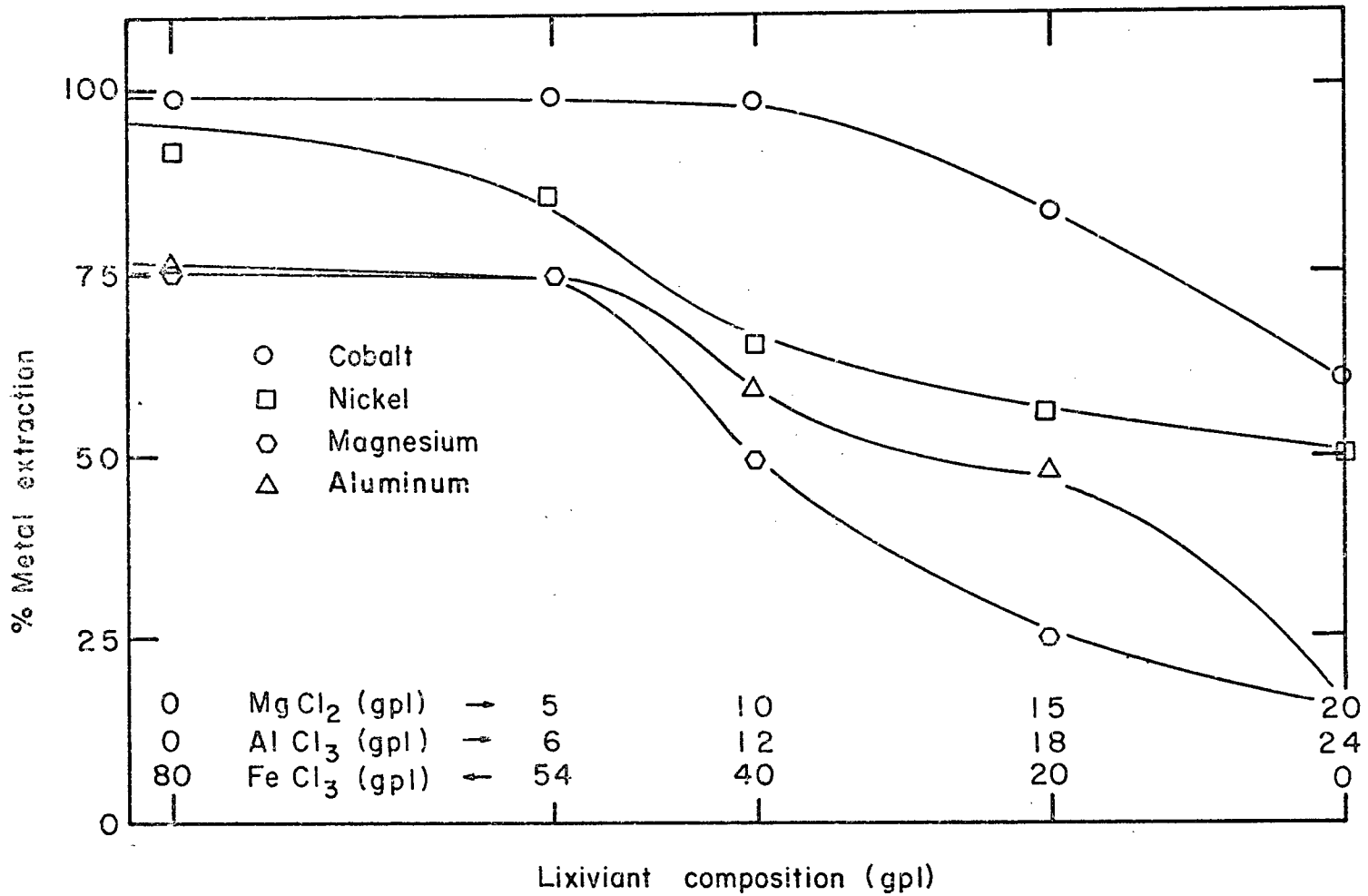

Figure 4.6 Metal extraction versus lixiviant composition at 423°K and a pulp density of 400 g/l

Table 4.9 Chemical Analysis of the Iron Residue From Each Stage

Element	Stages						Laterite Sample
	1	2	3	4	5	6	
	Weight Percentage						
Fe	57.5	57.5	56.2	48.2	45.4	44.7	44.55
Ni	0.02	0.17	0.38	0.54	0.64	0.7	1.25
Co	0.014	0.015	0.017	0.022	0.038	0.078	0.15
Cr	1.81	1.81[1]	-	-	-	-	2.26
Mn	0.10	0.10	0.11	0.13	0.25	0.41	1.08
Mg	0.34	0.44	0.49	0.95	1.72	2.07	2.31
Al	9.90	0.88	1.08	2.72	3.09	3.58	4.68
Si	2.46	-	-	-	-	-	2.65

[1]Estimated.

in concentration from 0.5M to 2M. Figures 4.7 (a), (b), (c) and (d) show SEM photomicrographs of hematite particles at 5000 times magnification, with particle size increasing from 0.8μm to 2μm. The particles were spherical and uniformly shaped, with a tendency to agglomerate.

4.7.2 Iron Residue from the Hydrothermal Treatment of Nickeliferous Laterite with Ferric Chloride Solutions

Hematite particles precipitated during leaching experiments, in which the lixiviant employed was ferric chloride, possessed highly etched surfaces. Particles were larger than those obtained from the hydrolysis of ferric chloride solution alone, and were irregular in shape.

The surfaces of particles immediately after precipitation may be somewhat different from those shown in the photomicrographs (Figure 4.8). There were indications of surface dissolution in particular directions corresponding to the direction of flow of the filtrate during filtration. This dissolution was particularly visible in photomicrographs of particles obtained through pressure filtration, which required an average of 30 minutes for completion. Such "laminar dissolution" was not apparent on particles recovered using the centrifugal technique.

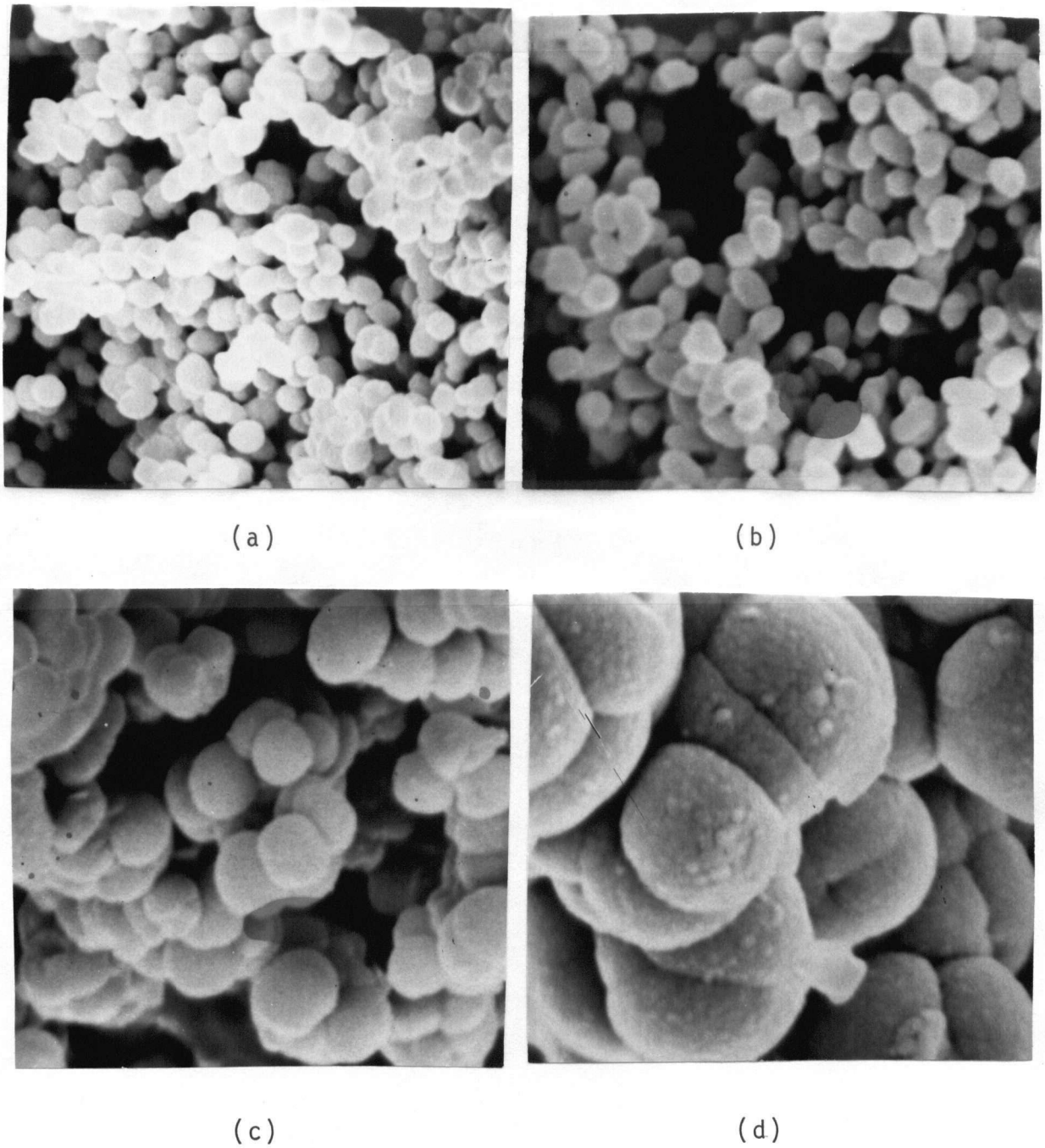

Figure 4.7 Hematite particles precipitated from ferric solutions at 423°K.

a) from 0.5M $FeCl_3$ (4000 x)
b) from 1M $FeCl_3$ (5000 x)
c) from 2M $FeCl_3$ (5000 x)
d) from 4M $FeCl_3$ (5000 x)

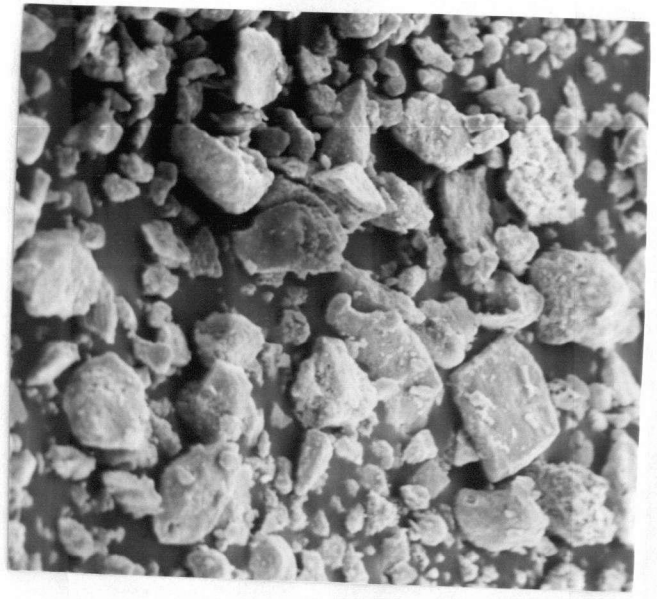

(a)

(b)

Figure 4.8 Iron residue obtained from the hydrothermal treatment of nickeliferous laterite with ferric chloride solutions.
a) from 2M $FeCl_3$, 433°K (380 x)
b) from 1M $FeCl_3$, 423°K (2000 x).

The cause of such redissolution was the reversal of the hydrolysis reaction on cooling. This behaviour was predicted by the thermodynamic information developed in Section 2.2.6, and evidenced by the loss of "free acid" during extended contact between residues and solution, as shown in Section 4.4.

Temperature and concentration of the ferric chloride solution employed did not have any significant effect on the morphology of the particles.

4.7.3 Iron Residue from the Hydrothermal Treatment of Nickeliferous Laterite with Ferric Chloride/ Hydrochloric Acid Solutions

The photomicrographs of Figure 4.9 show the surfaces of particles obtained from the above leaching experiments to be porous and highly etched. The particles were finer than those obtained from the preceding experiment. This reduction was attributed to a greater extent of redissolution of the precipitate on cooling.

4.8 Comparison of Nickeliferous Laterite and the Iron Residue by Electron Microanalysis

Figure 4.11 shows SEM X-ray analyser spectra taken for nickel-bearing laterite particles (see Figure 4.10) and iron residues precipitated under different leaching conditions.

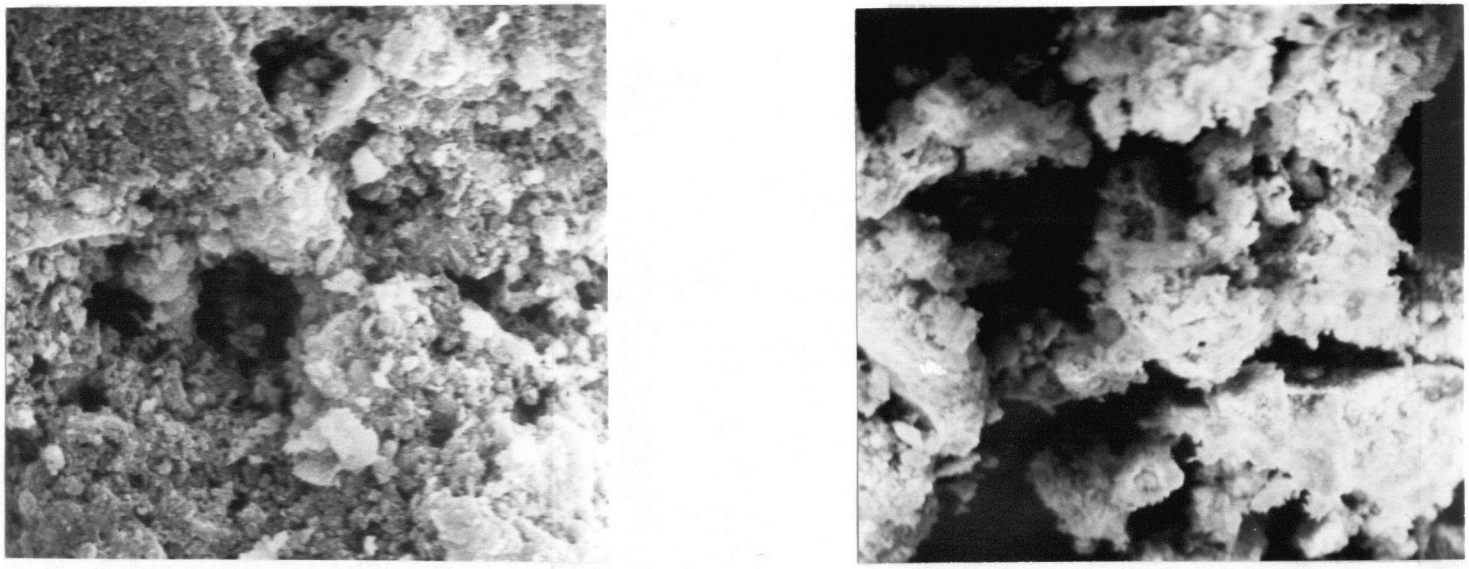

(a) (b)

Figure 4.9 Iron residue obtained from the hydrothermal treatment of nickeliferous laterite with ferric chloride / hydrochloric acid solutions.

a) from 1M $FeCl_3$, 3M HCl, at 423°K (2000 x)
b) from 1M $FeCl_3$, 2.5M HCl, at 423°K (800 x).

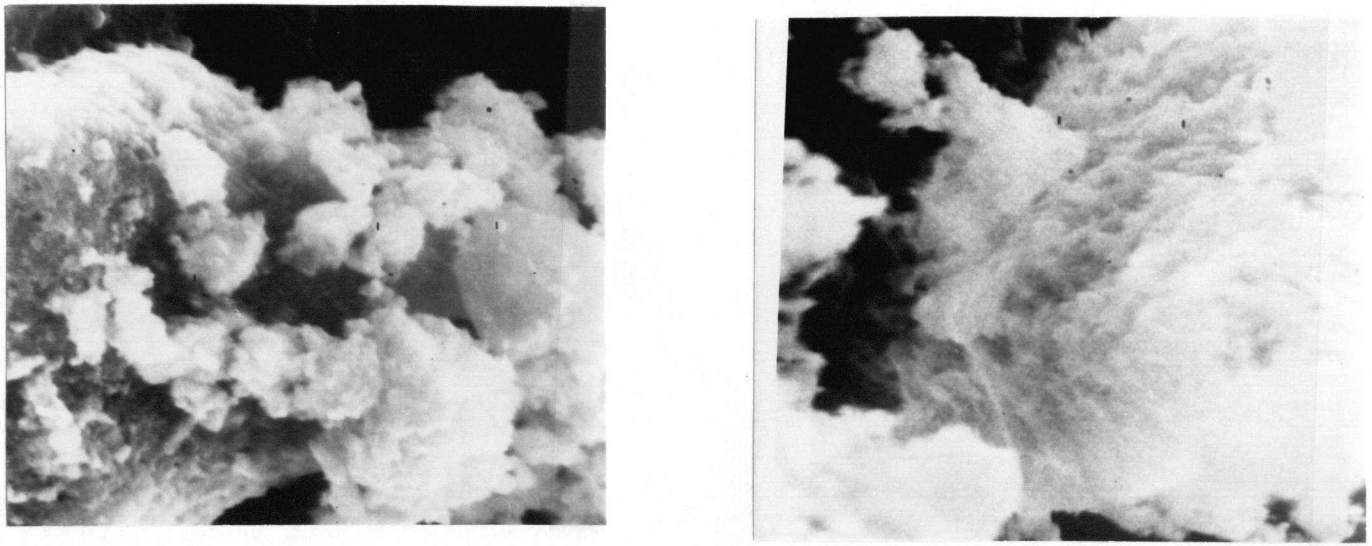

(a) (b)

Figure 4.10 a) Main nickel-bearing particles (of redish brown colour, 2000 x) white areas depict the mineral goethite; or quartz darker areas represent magnetic regions high in chromium.
b) Predominantly goethite (4000 x).

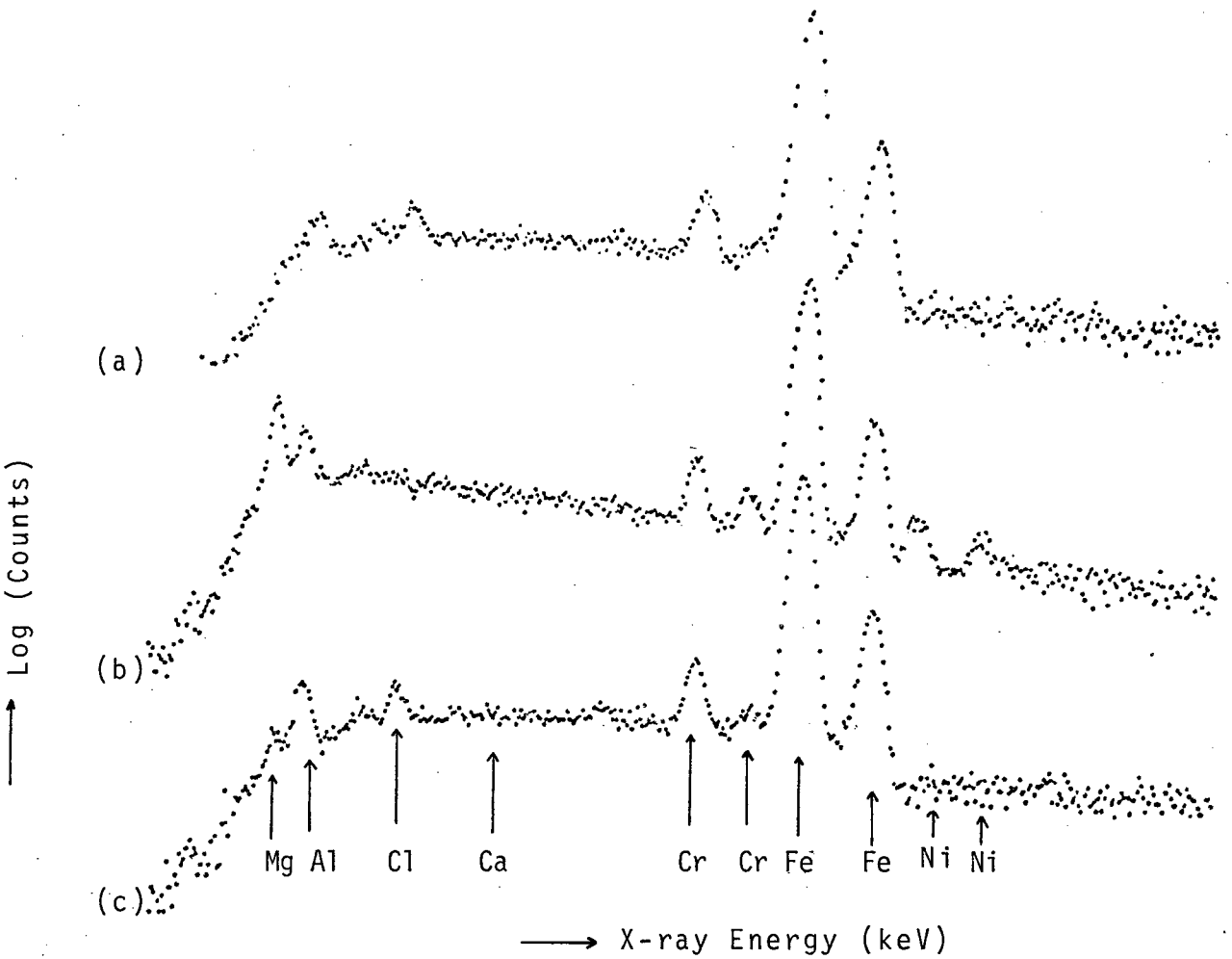

Figure 4.11 SEM x-ray analyser spectra for nickeliferous laterite and iron residue

(a) Iron residue from leach with 2M $FeCl_3$ at 453°K
(b) Nickeliferous laterite
(c) Iron residue from leach with 2M $FeCl_3$, 3M HCl, at 453°K

The spectra, containing 500,000 counts each, are shown together in order to accentuate their differences. The most striking feature illustrated is the disappearance of aluminium, magnesium and nickel from the laterite.

4.9 Comparison of Particles Found in Nickeliferous Laterite and the Iron Residue by Electron Microanalysis.

The photomicrographs shown in Figures 4.12 and 4.13 illustrate the various shapes and relative sizes of particles found in the laterite and iron residue. Figure 4.14 shows the corresponding SEM X-ray analyser spectra for some of those particles before leaching. Each spectra served to indicate the presence and relative abundance of elements without being truly-quantitative.

Quartz and chromite particles were insoluble under leaching conditions. However, there were indications of the removal of magnesium, aluminium and minor amounts of nickel from these particles. Some particles referred to as magnetic, contained a significant amount of magnesium, as distinct from chromite, which showed stronger peaks of chromium with less magnesium.

The spectra shown in Figure 4.15 illustrates the disappearance of magnesium, aluminium and nickel from particles after leaching.

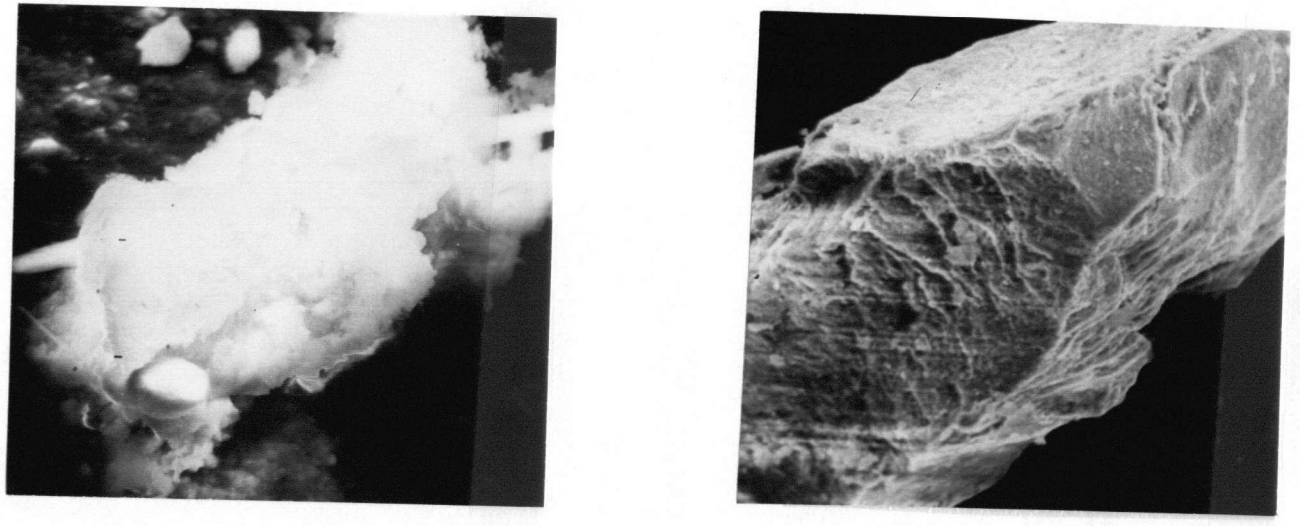

(a) (b)

Figure 4.12 a) Silicate particles after leaching in HCl/HNO_3 (200 x)
b) Pale-yellow silicate (400 x).

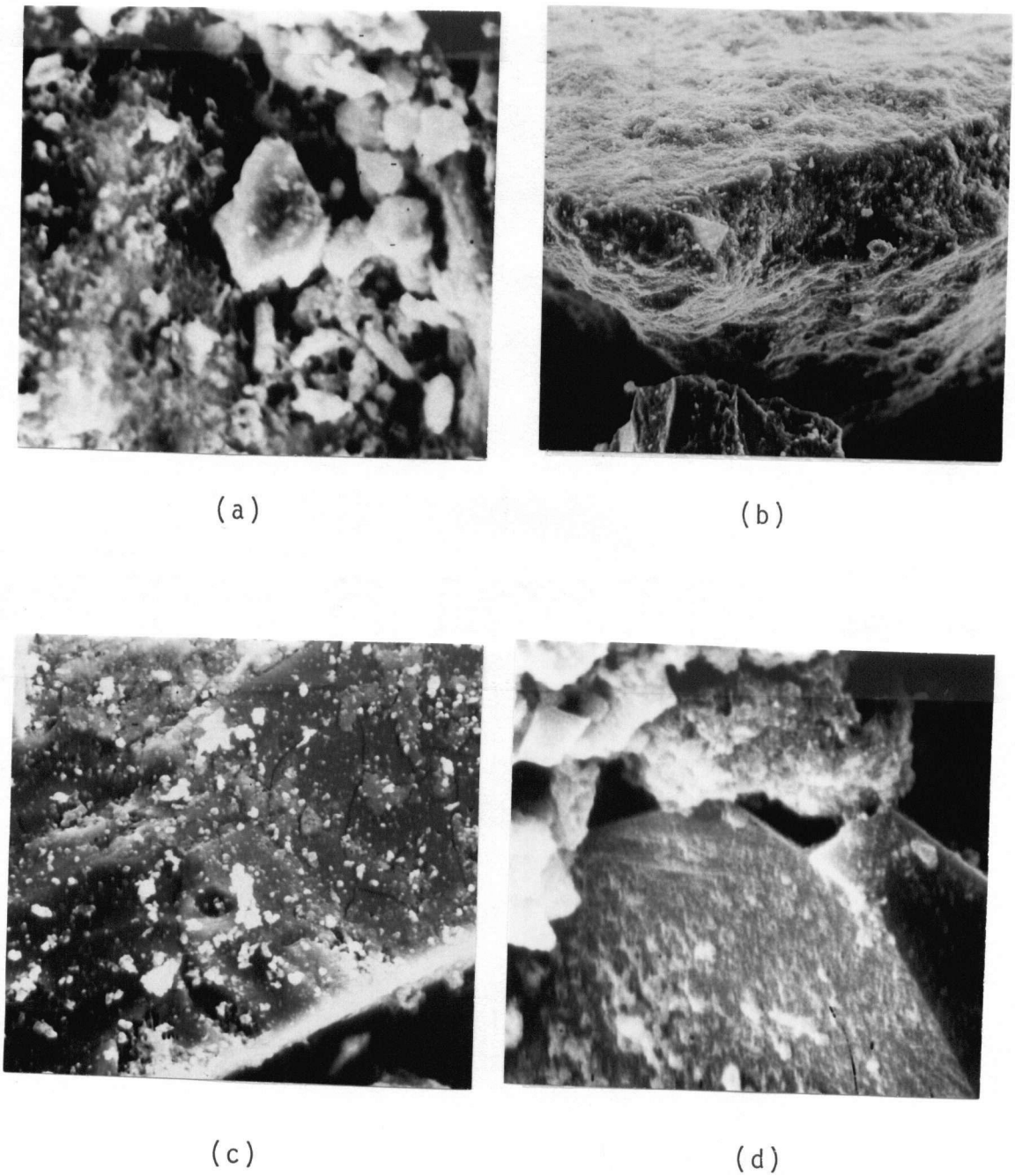

Figure 4.13 Magnetic particles found in nickeliferous laterite and the iron residue

a) magnetic particle before leaching (2000 x)
b) from 2M $FeCl_3$, at 453°K (340 x)
c) from 1M $FeCl_3$, 3.6HCl, at 423°K (1500 x)
d) from 2M $FeCl_3$, at 423°K (4200 x)

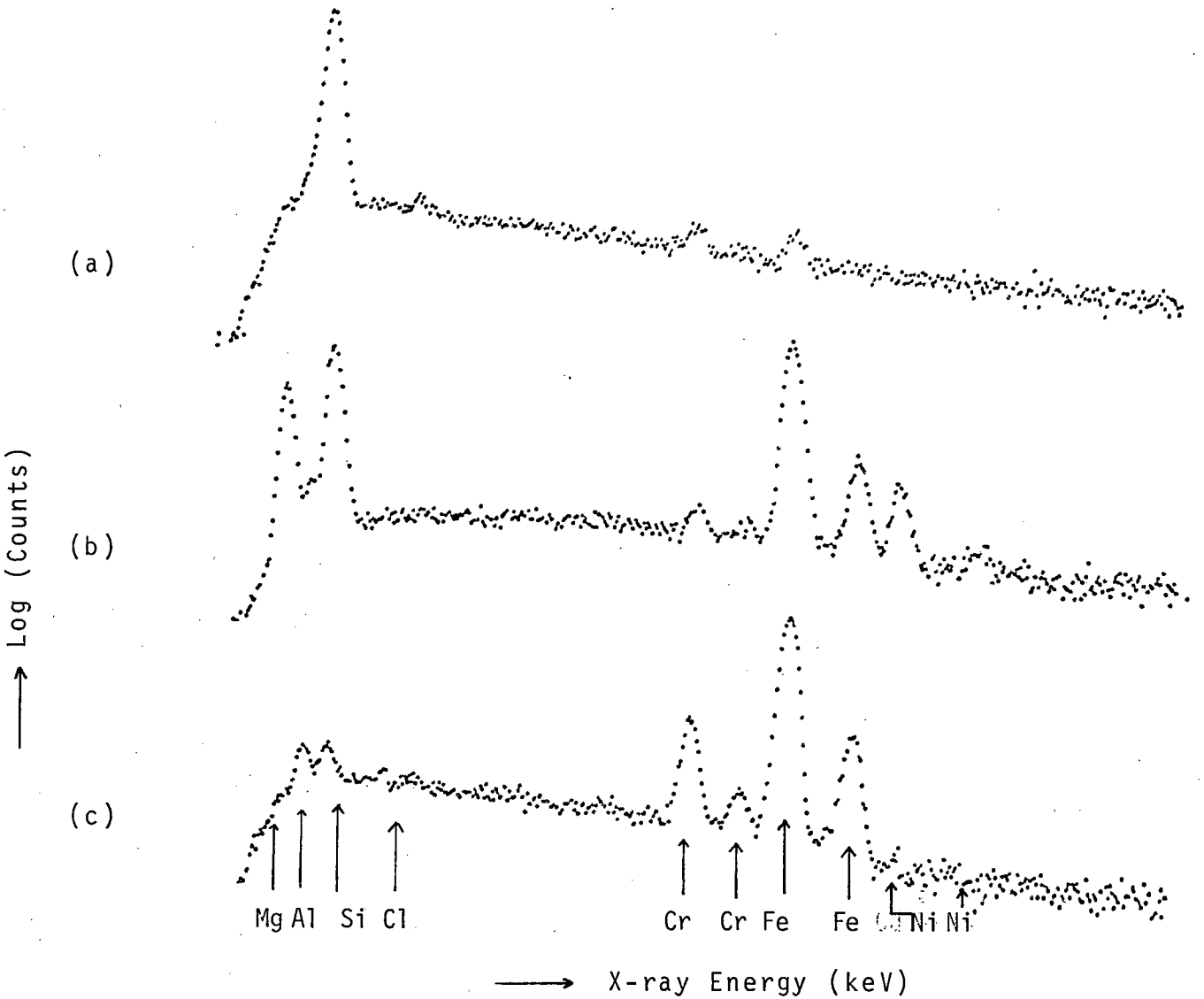

Figure 4.14 SEM x-ray analyser spectra for silicate and magnetic particles.
(a) Insoluble silicate
(b) Magnetic particle before leaching
(c) Chromite particle before leaching

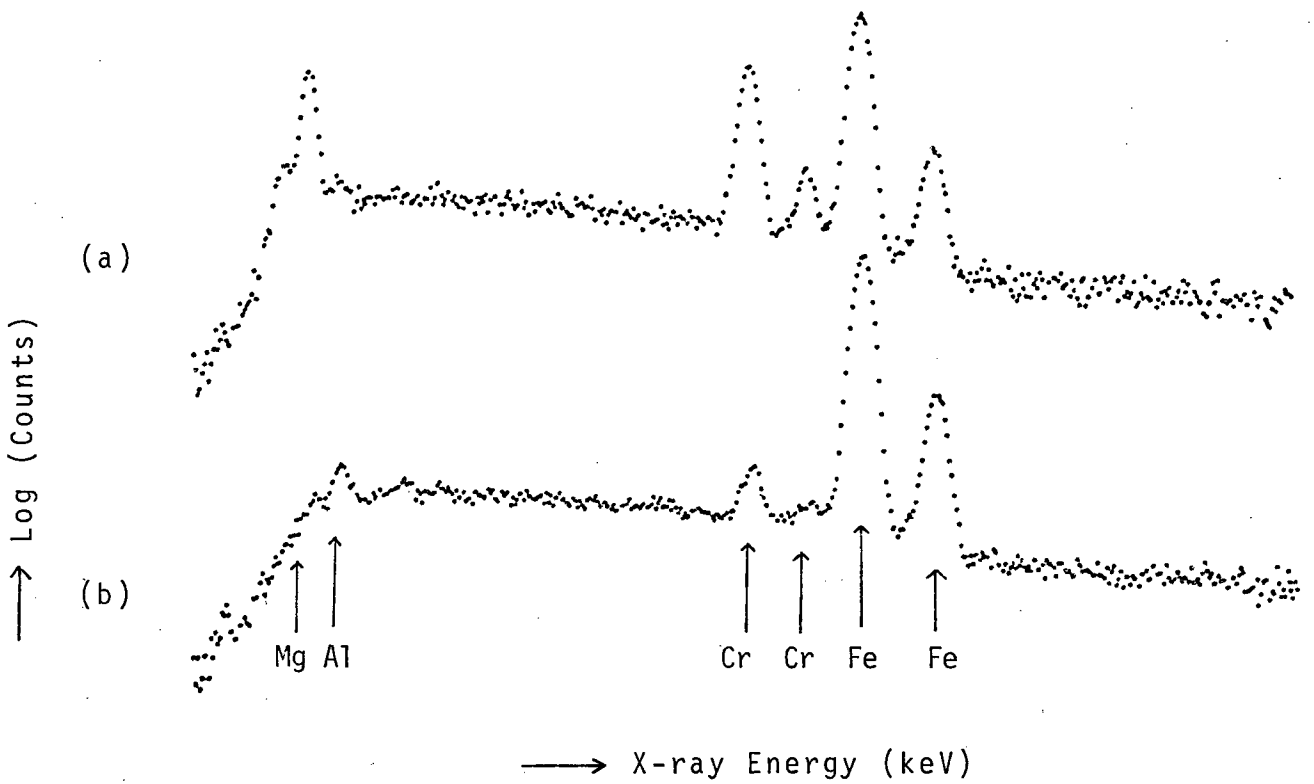

Figure 4.15 SEM x-ray analyser spectra for magnetic particles in the iron residue.

(a) Magnetic particle from leach with 1M $FeCl_3$, 3.6M HCl, at 423°K.

(b) Chromite particle

Chapter 5

DISCUSSION

5.1 Review of Leaching Results

It was established in the literature that the rate of iron extraction and therefore the rate of nickel extraction from goethite were proportional to the product of the hydrogen and chloride ion activities. However, leaching experiments done by the author indicate that extraction was more heavily dependent on chloride ion activity than hydrogen ion activity.

This was confirmed by leaching experiments in which a constant chloride ion concentration of 5.5N was employed. In one case, nickel extraction was 91 percent using a 5.5N hydrochloric acid solution, as compared to 94 percent using a ferric chloride/hydrochloric acid mixture of a total chloride concentration of 5.5N. The use of ferric chloride alone resulted in a nickel extraction of 96 percent. This concentration of chloride ion was employed, as it approximated the total amount of acid consumed in producing metal chlorides (see Section 4.4) at a pulp density of 400 g/l.

Magnesium and aluminium showed similar extraction behaviour, with approximately 75 percent of the metal extracted under most conditions of acid and ferric chloride concentrations.

Maximum extraction of cobalt and manganese was achieved under conditions previously described. This was however, to be expected, because of the close association of the two metal oxides.

5.2 The Significance of Acidity During Hydrolysis

It was shown in Chapter 2, that the log of the activity of ferric ion in equilibrium with hematite was a linear function of pH with a slope of minus 3. At a temperature of 423°K with a ferric ion activity of about 1M (approx. 56 g/l Fe) in solution, the pH due to hydrolysis of ferric chloride would be around -1.6. With reference to the Potential/pH diagram[51] for the $Fe - H_2O$ system at 423°K, ferric ions were observed to be in equilibrium with hematite at about the same pH.

However, these slurries were cooled below 353°K before filtration or centrifuge separation of solids was attempted, and at this lower temperature the equilibrium pH rises from -1.6 at 423°K to -1.04 at 333°K (see Table 2.2), a decrease

in free acid of a factor of 3.6. Redissolution of hematite is therefore anticipated, but because it is slow, it is more serious under conditions of long filtration times than under conditions of short centrifugal separation times.

5.3 Nature of the Iron Residue

Table 5.1 compares the chemical analysis of the iron residue, with that of currently marketed regular iron ore. Although the analyses compared favorably, the iron residue contained too much chromium for large-tonnage use by the Steel Industry. Other deleterious impurities such as nickel, magnesium and aluminium would also require separate consideration, reserved for the steelmaker.

Judging from the intensity of the peaks obtained in x-ray diffraction patterns, iron residues from leaches with ferric chloride solutions only may have been more crystalline than residues obtained from leaches in the presence of hydrochloric acid. However, the particle size of residues obtained in the presence of acid was smaller than that in the former. Therefore, it is not known at this point, whether the decrease in peak intensity was due to a decrease in particle size or reduced crystallinity.

The SEM X-ray analyser spectra of magnetic particles

Table 5.1 Comparison of Raw Materials[48] Used in the Iron and Steelmaking Industry

Analysis Dry %	Leached Nickeliferous Laterite	Iron Ore Pellets	Normal Iron Ore
Fe	57.5	64	59
Si	2.46	2.8	4.2
Al	0.90	0.27	0.8
Ca	-	-	0.2
Mg	0.34	0.3	0.12
Mn	0.10	0.2	0.5
Cr	1.81	0.01	0.01
Co	0.01	0.01	0.01
Ni	0.1	0.01	0.01

before and after leaching experiments showed very little extraction of chromium. It was apparent that nickel was more easily released from its lattice positions in goethite, and that the residual nickel occurred mainly as replacement atoms in silicate and chromite particles.

5.4 Hydrothermal Precipitation of Hematite in Supersaturated Ferric Chloride Solutions

5.4.1 Homogeneous Nucleation

Thermodynamically, a homogeneous supersaturated solution is in a metastable state and may remain so indefinitely. Before nuclei can grow, the system must overshoot a critical equilibrium point and pass into the region where ΔG_v (volume free energy) is negative. This equilibrium corresponds to a finite critical size, at which a nucleus if so formed can grow. Such nuclei can be formed spontaneously within the system due to statistical fluctuations in the free energy, or may be provided artificially by seeding.

The Gibbs free energy of nucleation is given by the expression:[52]

$$\Delta G = d^3 \Delta G_v + \alpha d^2 \gamma \qquad \ldots 5.1$$

where

d = The approximate diameter of the nucleus

d^3 = volume of the nucleus.

αd^2 = surface area.

α = A factor related to the shape of the nucleus (approximately 5 for homogeneous nucleation).

ΔG_v = Volume free energy (free energy/unit volume required to form the solid phase assumed to be in 1 piece; negative for supersaturated solutions).

γ = Surface free energy per unit area of the solid/liquid interface (always positive).

Assume γ and ΔG_v to be independent of d and α.

Equation 5.1 shows surface energy to be dependent on the square of the nuclear dimensions whereas the bulk free energy depends on its cube. Therefore, ΔG varies according to the absolute volume of the nucleus.

When the temperature is such that hematite is stable relative to ferric ions in solution, ΔG_v is negative. At small values of d, the surface term dominates and ΔG is positive; at large d the volume free energy term dominates because this is proportional to d^3. At a critical particle size d_c, ΔG passes through a maximum denoted by W. The value of W and d_c depend on ΔG_v and thus upon the temperature. Growth of hematite particles smaller than d_c leads to an increase in

the free energy and thus, there is a greater tendency for such particles to dissolve rather than grow; particles larger than r_c are stable because growth is accompanied by a decrease in free energy. Particles of diameter d_c are unstable having an equal chance of dissolving or growing.

Figure 5.1 graphically illustrates the free energy of formation of spherical embryos as a function of the diameter for a series of temperatures. At temperatures $T<T_E$, although there is a greater tendency for particles of diameters d_1, and d_2 to shrink, some may overcome the free energy barrier W due to thermal fluctuations and grow.

5.4.2 Growth of Nuclei[53]

The growth of precipitates from supersaturated solutions involves the formation of the precipitate phase, due to the transfer of atoms across an interface with a redistribution of solute species. In leaching experiments conducted, it was expected that the growth rate may have depended upon some or all of the following factors:

1) The detailed mechanism by which the interface propagated.
2) The rate of diffusion of the atoms in both phases.
3) Size effects: Small particles of a phase have a higher solubility than larger ones, due to differences in the radii of curvature of the interfaces.

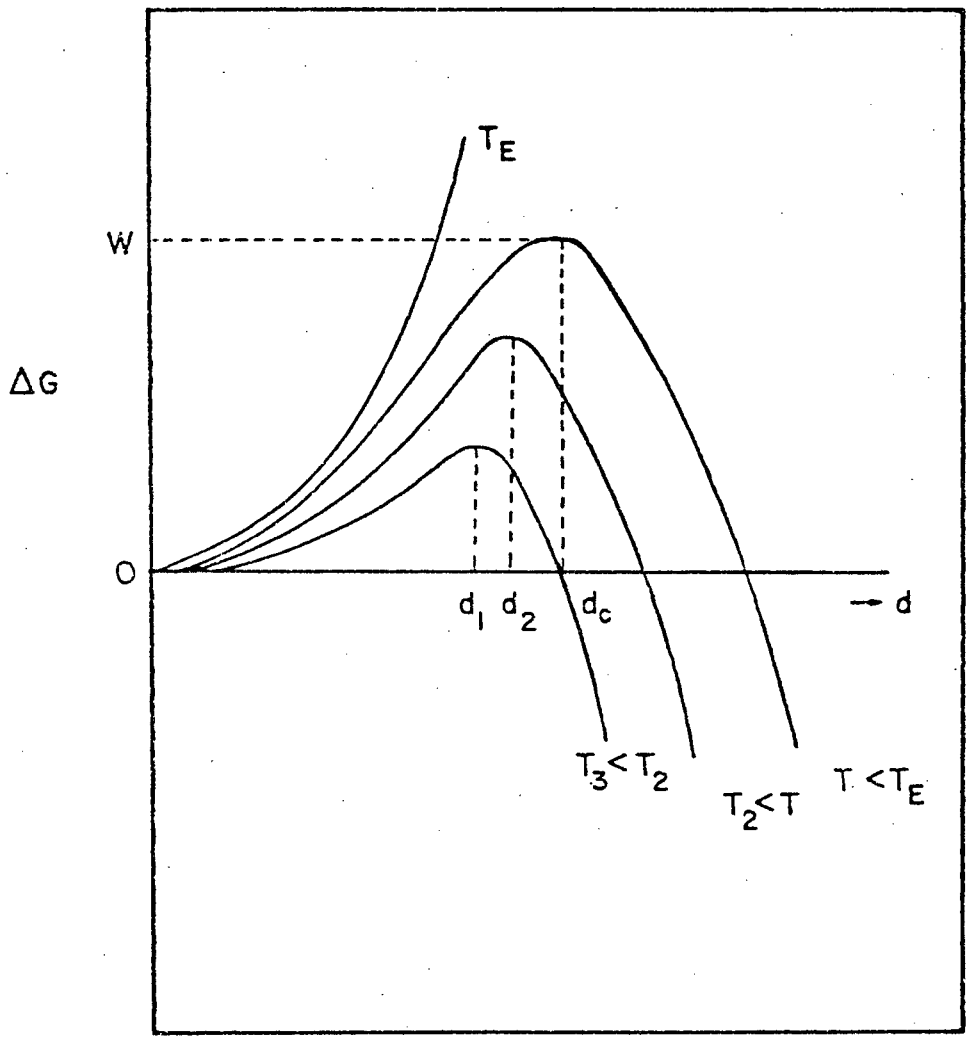

Figure 5.1 The free energy of formation of spherical embryos as a function of the diameter for a series of temperatures.

The heating of ferric chloride solution above 393°K results in a system containing mixed sizes of hematite nuclei (see Figure 5.1). A reduction in the overall free energy of the system could only be accomplished by a reduction in the total area of internal interfaces. This process requires diffusion of solute from regions close to small particles to regions around large ones (because the concentration of solute in the solution in equilibrium with a precipitate is larger for a small particle of precipitate than for a large one). Therefore, removal of solute from the solution near to small particles causes the latter to dissolve.

The coarsening of precipitates with increasing ferric chloride concentration as shown in Figure 4.7, may have been due to the gradual nature of the increase in the quantity of particles of varying sizes within each system. Furthermore, because small precipitate particles are more soluble, they dissolved to provide the solute for growth of the larger ones.

5.5 The Degree of Supersaturation for Hematite in a Goethite Saturated Solution.

The free energy per unit volume for nucleation can be expressed by:[54]

$$\Delta G_V = RT \ln \frac{a}{a_o} \qquad \ldots 5.2$$

where

a = activity of the dissolved matter

a_o = solubility at the actual temperature.

using $S = \frac{a}{a_o}$ (supersaturation ratio)

$$\Delta G_v = RT \ln S \qquad ...5.3$$

Equation 5.3 shows that an increase in the supersaturation ratio results in an increase of the free energy of the solution. This added free energy is then available to overcome the nucleation free energy barrier. If the free energy available from this source exceeds the critical maximum free energy for the most unstable nuclei in Figure 5.1, all sizes of nuclei become stable and the barrier for nucleation vanishes. Under these conditions nucleation is so fast that growth rates are almost irrelevant; this solution produces a large number of very small particles.

In leaching experiments conducted, it appeared that the goethite dissolved rapidly to produce sufficiently supersaturated solutions with the inherent fast rate of nucleation. A large amount of very fine hematite particles precipitated rapidly under conditions where growth was limited because of the large interfacial area generated by nucleation. Such particles receive a limited amount of precipitating solute which resulted in fine precipitates and poor filterability.

However, equation 5.3 indicates that if a lower degree of supersaturation can be established during goethite dissolution (and therefore, a decrease in the free energy of formation ΔG), hematite particles will not nucleate spontaneously. Those that do surmount the free energy barrier and grow will become much larger than under spontaneous nucleation conditions. Improved filterability can therefore be expected.

By considering the theoretical equilibrium pH at several activities of ferric ion as described in sections 2.2.5 to 2.2.7, the free energy for the precipitation of hematite from a goethite saturated solution can be calculated. Values of ferric ion activity in equilibrium with hematite were calculated at room temperature using the relationship:

$$pH = \frac{1}{3}\left[-\log K - \log a_{Fe^{3+}}\right]$$

Assuming total dissolution of goethite, the associated pH, were first calculated, employing the equilibrium constant for the Fe^{3+} - FeOOH equilibrium at 423°K. These pH values were then used to calculate the activity of ferric ion in equilibrium with hematite, this time, employing the equilibrium constant for the Fe^{3+} - Fe_2O_3 equilibrium at the same temperature. The results obtained are shown below:

Log $[Fe^{3+}]$ (from dissolved FeOOH)	pH	Log $[Fe^{3+}]$ (in equilibrium with Fe_2O_3)	$\frac{[Fe^{3+}]}{[Fe^{3+}]}$ (Hematite) (Goethite)
0	-1.48	0.36	2.29 x
-1	-1.15	-1.35	2.24 x
-2	-0.81	-2.37	2.34 x

Using equation 5.3,

$$\Delta G^{\circ}_{R_{(Max.)}} = RT \ln 2.3$$

$$= 700 \text{ calories } MOL^{-1} Fe^{3+} \text{ at } 423^{\circ}K.$$

These data make it clear that 700 calories per mole Fe^{3+} are available from a saturated solution of goethite to overcome the nucleation free energy barrier of hematite. This value is probably high enough to cause spontaneous nucleation of hematite yielding very fine, poorly filterable precipitates.

Chapter 6

CONCLUSION

The results of the leaching experiments indicate that a promising process might be devised for the hydrothermal treatment of nickeliferous laterite with ferric chloride solutions. Direct ore attack obviates the need for prior pyro-metallurgical reduction, but at the expense of unit operations to recover magnesium, aluminium, manganese, and chromium.

Of the chlorides present in solution, iron, aluminium and magnesium hydrolyze readily at moderate temperatures. Hydrochloric acid can therefore be recovered from the mother liquor by hydrolysis in an Aman-type reactor (AMAN, J. 1956, 1958), and recycled in the system.

Close scrutiny of the leaching results obtained in the simulation of a continuous leaching circuit, indicate that two stages of leaching would have to be utilized, in order to obtain at least 90 percent nickel extraction.

Owing to the amorphous and friable nature of the precipitated residue, filtration was extremely difficult. In order to thoroughly wash the residue, it was necessary to repulp at least twice. This virtually removed all of the chlorides. In industrial practice, an economic balance would have to be struck between the cost of evaporating excess wash water and the loss of chlorides in the residue.

It appears that the iron ore residue would not meet acceptable specifications with regard to chromium, and probably nickel, without further beneficiation. Furthermore, recovery of, at most, half of the ore's chromium content by physical means is a possibility but of doubtful industrial merit.

The marked difference in the morphology of hematite precipitated from ferric chloride reagent, and that of the iron residue was due to the following:

1) Dissolution of the precipitate on cooling.
2) Rapid precipitation under super-saturated conditions.

These conditions resulted in a precipitate of poor filterability. It appears however, that once conditions of precipitation can be controlled, some improvement in particle size and/or shape may be expected. This should result in better filterability of the iron residue.

Chapter 7

SUGGESTIONS FOR FUTURE WORK

7.1 Improvement in Experimental Procedure

In this investigation, leaching was restricted to batch runs using a small titanium autoclave. Such runs had the drawback that a significant amount of hydrolysis occurred in the heating up period, which took about 20 minutes. It was therefore difficult to assess the effect of variables such as retention time and temperature from such experiments.

A continuous experimental arrangement[36] should therefore be devised, in which the leach solution to be hydrolysed is pumped continuously into a heated autoclave. The reacted slurry is allowed to overflow continuously into a receiving vessel, the contents of which may be periodically adjusted and recycled. With such back mixing, hematite nuclei would be in a regime suitable for continued growth, because conditions of severe supersaturation can be avoided. Lower levels of supersaturation will lead to slow nucleation and coarse precipitates.

REFERENCES

1 Queneau, P.E. and Roorda, H.J. Cobalt and the Nickeliferous Limonites. De Ingenéur, Vol. 83, No. 28, (1971), pp. 1-9.

2 Bolt, J.R., Queneau, P.E. The Winning of Nickel. D. Van Nostrand Co., Princeton, N.J., (1967).

3 Stevens, L.G., Goeller, L.A., MIller, M. "The UOP Nickel Extraction Process" CIMM, 14th Annual Conference Edmonton, Alberta, Canada, (1975).

4. Weege, R.J., Beres, W.J., "The Exploration and Development of Nickel Laterites" AIME Annual Meeting, Denver, Colorado, Feb. 27, 1978.

5 Posnjack, E. and Merwin, H.E. Am. J. Sc. Vol. 47, (1919), pp.311-348.

6 Kulp, J.L., and Tites, A.F., Am. Miner. Vol. 36, (1951), pp. 23-44.

7 White-Howard, F.B. Nickel - A Historical Review. D. Van Nostrand Co., Inc., New York, (1963), p.352.

8 Mineral Commodity Profiles, May 1979.
United States Department of the Interior.

9 Engineering and Mining Journal, March 1981, p. 137.

10 Cornwall, H.R. Nickel Changes in United States Mineral Resources, U.S. Geol. Survey Prof. Paper 820, (1973), pp. 437-442.

11 Roorda, H.J., Queneau, P.E. M.I.M Manuscript, June 1973.

12 Agarwal, J.C., Reddy, B.J. Role of Cobalt in Industrial Society. CIM Report 10th Annual Hydromet Meeting, Edmonton, Alberta, Oct. 1980.

13 Cuban American Nickel, Engineering and Mining Journal, 158, Vol. 79, (1957).

14 Mancke, E.B., U.S. Patent, 2, 762, 703 (1956).

15 Wescott, E.H., ibid. 2, 036, 664 (1936).

16 Graham, M.E., Reed, R., and Cameron, J.R. ibid. 2, 766, 115 (1956).

17 Van Nes, C.L. Dutch Patent Application 193, 612 (1955) N.O. 89510 (1958).

18 Caron, M.H., ibid. 1, 487, 145 (1924).

19 Heertjes, P.M. and Van Nes, C.L. Recovery of Nickel and Cobalt from Lateritic Iron Ores. Recl. Trav. Chim. Pays-Bas Belg. Vol. 79, (1960), pp. 593-604.

20 Seimens, R.E., Corrick, J.D. "Process for Recovery of Nickel, Cobalt and Copper from Domestic Laterites," Mining Congress Journal, January, 1977, pp. 29-34.

21 Wilson, F. Min. Eng. Vol. 10, (1958), pp. 563-565.

22 Anon. Report on Moa Bay. New York Times, 5 Feb. 1968.

23 Rice, N.M., Strong, L.W. The Leaching of Laterite Nickel Ores in Hydrochloric Acid. CIM Quarterly, Vol. 13, No. 3, 1974.

24 Goldztaub, S. Compt. Rend. Acad. Scl. URSS Vol. 195, (1932), p. 264.

25 Jurinak, J.J. Journal of Colloid Science Vol. 19, (1964), pp. 477-487.

26 Bath, M.D., M.A.Sc. Thesis, Dept. of Metallurgy, U.B.C. (1968).

27 Roach, G.I.D. M.A.Sc. Thesis, Dept. of Metallurgy, U.B.C. (1968).

28 Surana, V.S. M.A.Sc. Thesis, Dept. of Metallurgy, U.B.C. (1969).

29 Devuyst, E. Ph.D. Thesis, Dept. of Metallurgy, U.B.C. (1973).

30 Azuma, K. and Kametani, H. Trans. AIME., Vol. 230, (1964), p.853.

31 Parks, G.A. and De Bruyn, P.L. J. Phys. Chem., Vol. 66, (1962), p. 967.

32 Ahmed, S.M. and Marksimov, D. Studies of the Double Layer at the Oxide-solution Interface, Department of Energy, Mines and Resources, Mines Branch, Ottawa, 1968.

33 Criss, C.M. and Cobble, J.M. The Thermodynamic Properties of High Temperature Aqueous Solutions. IV : Entropies of the Ions up to 200° and the Corresponcence Principle, J. Amer. Chem. Soc. Vol. 86, (1964), pp. 5385-5390.

34 Criss, C.M. and Cobble, J.M. The Thermodynamic Properties of High Temperature Aqueous Solutions V : The Calculation of Ionic Heat Capacities up to 200°, Entropies and Heat Capacities Above 200°, J. Amer. Chem. Soc., Vol. 86, (1964), pp. 5390-5393.

35 Robins, R.G. J. Inorg. Nucl. Chem. Vol. 29, (1967) pp. 431-435.

36 Haigh, C.J. Hydrolysis of Iron in Acid Solutions Proc. Aust. Inst. Min. Met., Sept., 1967.

37 Lietzke, M.H. and Stoughton, R.W. J. Phys. Chem. Vol. 63, (1959), pp. 1183, 1186, 1188, 1190, 1984.

38 Cobble, J.W. J. Amer. Chem. Soc. Vol. 86, (1964), p. 5394.

39 Meissner, Kusik and Tester. AICHE Journal Vol. 18, No. 3, May 1972, p. 661.

40 Feitknecht, W. and Schindler, P. Solubility Product of Metal Oxides. Pure Appl. Chem. Vol. 6, (1963), pp. 130-199.

41. Biedermann, G. and Schindler, P. ACTA Chem. Scand. Vol. 11, pp. 731-740.

42 Weiser, H.B. Inorganic Colloid Chemistry Vol. 11, (1935), p. 40.

43 Posnjak, E. and Merwin, H.E. The System $Fe_2O_3—SO_3—H_2O$, J. Amer. Chem. Soc. Vol. 44, (1922), pp. 1965-1993.

44. Tunell, G. and Posnjack, E. The Stability Relations of Goethite and Hematite (Discussions) - Econ. Geol., Vol. 26, (1931), pp. 337-343.

45 Gruner, J.W. The Stability Relations of Goethite and Hematite (Discussion) - Econ. Geol., Vol. 26, (1931), pp. 442-445.

46 Smith, F.G. and Kidd, D.J. Am. Mineralogist, Vol. 34, (1949), p. 403.

47 Katsurai, T. and Watanabe, T. The Structure of Iron Oxide Prepared by the Autoclave Treatment. Sci. Pap. Inst. Phys. Chem. Res., Tokyo, Vol. 13, pp. 89-92.

48 Queneau, P.E. Cobalt and the Nickeliferous Limonites Doctoral Thesis, University of Delft, 1971, p. 254.

49 Kelley, K.K. U.S. Bureau of Mines Bulletin 476 U.S. Government Printing Office, Washington, D.C., 1949.

50 Barner, H.E. and Scheurman, R.V. Handbook of Thermochemical Data for Compounds and Aqueous Species 1978.

51 Biernat, R.J. and Robins, R.G. High Temperature Potential/pH Diagrams for the Iron-Water System Electrochimica Acta, Vol. 17, (1972), pp. 1261-1283.

52 Cottrell, A. An Introduction to Metallurgy, Second Edition, SI Units.

53 Burke, J. The Kinetics of Phase Transformations in Metals.

54 Nielsen, A.E. Kinetics of Precipitation Pergamon.

Appendix A

CRISS AND COBBLE CALCULATIONS

Appendix A

A.1 The Effect of Temperature on Thermodynamic Parameters

1) Consider the Effect of Temperature on Enthalpy of a Single Species Involved in a Reaction

$$C_p = \left(\frac{dH}{dT}\right)_p$$

and

$$\Delta H = \int_{T_1}^{T_2} \bar{C}_p \, (T_2 - T_1)$$

$\bar{C}_p$ average being used due to the fact that C_p is not normally constant between the temperatures.

2) The Effect of Temperature on Entropy

$$dS_p = C_p \frac{dT}{T}$$

$$\Delta S_p = \int_{T_1}^{T_2} C_p \frac{dT}{T}$$

and

$$\Delta S_p = \bar{C}_p \ln \frac{T_2}{T_1}$$

3) The Effect of Temperature on Free Energy

At temperature, T_1 $G_1 = H_1 - T_1S_1$

At temperature, T_2 $G_2 = H_2 - T_2S_2$

therefore,

$$\Delta G = \Delta H - \left(T_2-T_1\right) S_1 - T_2\Delta S$$

where ΔH and ΔS have already been defined.

Considering now the change in free energy of a reaction in going from 298°K to temperature T.

$$\Delta G^\circ_T - \Delta G^\circ_{298} = \Delta H^\circ_T - \Delta H^\circ_{298} - (T\Delta S^\circ_T - 298\Delta S^\circ_{298}) \qquad \ldots(a)$$

however,

$$\Delta S^\circ_T - \Delta S^\circ_{298} = \int_{298}^{T} \Delta C^\circ_p \, d\,(\ln T)$$

therefore,

$$T\Delta S^\circ_T = T\Delta S^\circ_{298} + T\int_{298}^{T} \Delta C^\circ_p \, d\,(\ln T) \qquad \ldots(b)$$

now

$$\Delta H^\circ_T - \Delta H^\circ_{298} = \int_{298}^{T} \Delta C^\circ_p \, dT \qquad \ldots(c)$$

by substituting (c) and (b) into (a) we get:

$$\Delta G^\circ_T = \Delta G^\circ_{298} + \int_{298}^{T} \Delta C^\circ_p \, dT - T\Delta S^\circ_{298} - T \int_{298}^{T} \Delta C^\circ_p \, d(\ln T) + 298\,\Delta S^\circ_{298}$$

by rearranging,

$$\Delta G^\circ_T = \Delta G^\circ_{298} - \Delta T \Delta S^\circ_{298} + \int_{298}^{T} \Delta C^\circ_p \, dT - T \int_{298}^{T} \Delta C^\circ_p \, d(\ln T) \qquad \ldots(d)$$

The detailed variation of C°_p with temperature is not usually well known, but satisfactory estimates may be obtained from average values of C_p over the temperature range. Therefore, using average values of C_p, equation (d) becomes:

$$\Delta G^\circ_T = \Delta G^\circ_{298} - \Delta T \Delta S^\circ_{298} + \Delta \bar{C}_p \Big]_{298}^{T} \Delta T - T \Delta \bar{C}^\circ_p \Big]_{298}^{T} \ln T/298 \qquad \ldots(e)$$

where

$$\Delta T = T - 298$$

ΔG° and ΔS° values are well established by experiment at 298°K. Therefore, in order to solve equation (e), it is necessary to estimate $\Delta \bar{C}_p \Big]_{298}^{T}$.

A.2 Criss and Cobble Entropy Correspondence Principle

Criss and Cobble[33,34] using data at different temperatures established a correspondence principle, whereby the entropy at a given temperature, $S^{\circ}_{T_2}$ can be expanded about a reference temperature, T_1 such that:

$$S^{\circ}_{T_2} = a_{T_2} + b_{T_2} S^{\circ}_{T_1} + C_{T_2} (S^{\circ}_{T_1})^2 + d_{T_2} (S^{\circ}_{T_1})^3$$

It was shown that a standard state can be chosen at every temperature, such that the partial molal entropies of one class of ions in solution at that temperature are linearly related to the corresponding entropies at some reference temperature.

$$S^{\circ}_{T} = a_T + b_T S^{\circ}_{298}$$

S°_{298} in the above expression is expressed in absolute units, which is defined as:

$$S^{\circ}_{298\ \text{Abs}} = S^{\circ}_{298\ \text{Conventional}} - 5.0(Z)\ \text{Cals Mol}^{-1}\ \text{Deg}^{-1}$$

where Z = Ionic Charge

In a subsequent publication, the following procedure was adopted:

When the entropy of an ion is known (or can be accurately predicted at two temperatures, then the average value of the heat

capacity $\bar{C}_p\Big]_{T_1}^{T_2}$ can be calculated

$$S_T^\circ - S_{298}^\circ = \bar{C}_p\Big]_{298}^{T_2} \ln T/298$$

$$a_T + (b_T - 1)\, S_{298}^\circ = \bar{C}_p\Big]_{298}^{T} \ln T/298$$

therefore,

$$\bar{C}_p^\circ\Big]_{298}^{T} = \frac{a_T - S_{298}^\circ (1-b_T)}{\ln T/298}$$

and

$$\bar{C}_p^\circ\Big]_{298}^{T} = \alpha_T + \beta_T S_{298}^\circ$$

where

$$\alpha_T = \frac{a_T}{\ln T/298}$$

and

$$\beta_T = \frac{-[1-b_T]}{\ln T/298}$$

The heat capacity constants α_T, β_T of simple cations, anions, and oxyanions etc. at various temperatures are shown in Table A.1. Therefore, from calculations of $\bar{C}_p^\circ\Big]_{298}^{T}$, it is possible to determine $\Delta C_p^\circ\Big]_{298}^{T}$, which can be inserted in equation (e).

Table A.1 Best Values of $a_t, b_t, \alpha_t, \beta_t$ and $S_t^\circ(H^+)$ at Several Temperatures

Temperature		298°K	333°K	373°K	423°K	473°K
$S_t^\circ(H^+)$		-5	-2.5	+2.0	+6.5	(11.1)
$\bar{C}_p]_{298}^T(H^+)$		0	23	31	33	(35)
Cations:	a_t	0	3.9	10.3	16.2	(23.3)
	b_t	1.000	0.955	0.876	0.792	(0.711)
	a_t	-	35	46	46	(50)
	β_t	-	-0.41	-0.55	-0.59	(-0.63)
Anions	a_t	0	-5.1	-13.0	-21.3	(-30.2)
	b_t	1.000	0.969	1.000	0.989	(0.981)
	a_t	-	-46	-58	-61	(-65)
	β_t	-	-0.28	0.000	-0.03	(-0.04)
Oxy anions	a_t	0	-14.0	-31.0	-46.4	(-67.0)
i.e. $CO_3^=$	b_t	1.000	1.217	1.476	1.687	(2.020)
$SO_4^=$	a_t	-	-127	-138	-133	(-145)
$C_2O_4^=$	β_t	-	1.96	2.24	2.27	(2.53)
$PO_4^=$						
Acid Oxyanions	a_t	0	-13.5	-30.3	(-50)	(-70)
i.e. HCO_3^-	b_t	1.000	1.380	1.894	(2.381)	(2.960)
$H_2PO_4^-$	a_t	-	-122	-135	(-143)	(-152)
$HPO_4^=$	β_t	-	3.44	3.97	(3.95)	(4.24)
HSO_4^-						

Table A.2 Standard Free Energies, Entropies and Partial Molal Ionic Heat Capacities Adopted for Species Participating in Reactions Considered in the Fe^{3+}—H_2O System

Species	333°K $\bar{C}^{\circ}_{p\,298}^{T}$	373°K $\bar{C}^{\circ}_{p\,298}^{T}$	423°K $\bar{C}^{\circ}_{p\,298}^{T}$	473°K $\bar{C}^{\circ}_{p\,298}^{T}$	S°_{298}	G°_{298} K.Cals
H^+	23	31	33	35	-5	0
Fe^{+++}	69.9	92.8	96.2	103.6	-85.1	-1.1
H_2O	18.04	18.04	18.15	18.15	16.7	-56.7
Fe_2O_3	26.5	27.9	29.4	30.7	21.5	-177.4
FeOOH	19.0	20	21.5	22	22	-117
$Fe(OH)_3$	20	20	20	20	25.5	-166.5

A.3 Sample Calculation for the Estimation of Thermodynamic Data at Elevated Temperatures

Hydrolysis of Hematite

$$Fe^{3+} + \frac{3}{2} H_2O = \frac{1}{2} Fe_2O_3 + 3H^+$$

At 298°K, the standard free energy change for the reaction is calculated using the G°_{298} value for each species.

$$G^\circ_{298} = \frac{1}{2}\left[(-177.4) + 3(0)\right] - \left[-1.1 + \frac{3}{2}(-56.7)\right]$$

$$= -2550 \text{ cals}$$

Similarly, the standard entropy change for the reaction is calculated from the S°_{298} value for each species.

$$\Delta S^\circ_{298} = \left[\frac{1}{2}(21.5) + 3(-5)\right] - \left[-85.1 + \frac{3}{2}(16.7)\right] = 55.8 \text{ e.}$$

$$\Delta C_p\Big]_{298}^{333} = \left[\frac{1}{2}(26.5) + 3(23)\right] - \left[69.9 + \frac{3}{2}(18.04)\right] = 15 \text{ Cal Mol}^{-1}{}^\circ\text{K}^{-1}$$

$$\Delta C_p\Big]_{298}^{373} = \left[\frac{1}{2}(27.9) + 3(31)\right] - \left[92.8 + \frac{3}{2}(18.04)\right] = -13 \quad "$$

$$\Delta C_p\Big]_{298}^{423} = \left[\frac{1}{2}(29.4) + 3(33)\right] - \left[96.2 + \frac{3}{2}(18.15)\right] = -10 \quad "$$

$$\Delta C_p\Big]_{298}^{473} = \left[\frac{1}{2}(30.7) + 3(35)\right] - \left[103.6 + \frac{3}{2}(18.15)\right] = -10 \quad "$$

The free energy changes at temperatures 333°, 373°, 423° and 473°K are then calculated using equation (e).

$$\Delta G^{\circ}_{T} = G^{\circ}_{298} + \bar{C}^{\circ}_{p}\Big]^{T}_{298}(T-298) - S^{\circ}_{298}(T-298) - T\,\bar{C}^{\circ}_{p}\Big]^{T}_{298} \ln \frac{T}{298}$$

$$\Delta G^{\circ}_{333} = -2550 + [-15x35] - [55.8x35] - [222x-15x.111] = -4774 \text{ Cals}$$

$$\Delta G^{\circ}_{373} = -2550 + [-13x75] - [55.8x75] - [373x73x.2245] = -6621 \text{ Cals}$$

$$\Delta G^{\circ}_{423} = -2550 + [-10x125] - [55.85x125] - [423x-10x.35] = -9295 \text{ Cals}$$

$$\Delta G^{\circ}_{473} = -2550 + [-10x175] - [55.85x175] - [473x-10x.462] = -11880 \text{ Cals}$$

The summary of available measured data on free energy and entropy of species participating in the hydrolysis reactions considered, is shown in Table A.2. Partial molal ionic heat capacities were calculated using;

$$\bar{C}^{\circ}_{p}\Big]^{T}_{298} = \alpha_T + \beta_T S^{\circ}_{298}$$

and utilizing values of α_T and β_T, which are given in Table A.1.

Table A.3 shows the average heat capacities over the temperature ranges considered, for each hydrolysis reaction. These values were utilized in equation (e), for the computation of the free energy, ΔG°_{T} of each reaction at the specified temperature. The summary of the computed free energies

of each reaction is shown in Table A.4

Thermodynamic data were considered for the following equilibria reactions.

$$Fe^{+++} + \frac{3}{2} H_2O \rightleftharpoons \frac{1}{2} Fe_2O_3 + 3H^+ \quad (1)$$

$$Fe^{+++} + 2H_2O \rightleftharpoons FeOOH + 3H^+ \quad (2)$$

$$Fe^{+++} + 3H_2O \rightleftharpoons Fe(OH)_3 + 3H^+ \quad (3)$$

Table A.3 Summary of Average Heat Capacities Over the Ranges of 298°K to Upper Limits of 333°, 373°, 423° and 473°K (Estimated by the Correspondence Principle)

Reaction	ΔS°_{298} e.u.	ΔC_p Ave Cal Mol^{-1} Deg^{-1}			
		$\Delta \bar{C}^{\circ}_p \Big]_{298}^{333}$	$\Delta \bar{C}^{\circ}_p \Big]_{298}^{373}$	$\Delta \bar{C}^{\circ}_p \Big]_{298}^{423}$	$\Delta \bar{C}^{\circ}_p \Big]_{298}^{473}$
(1)	55.8	-15	-13	-10	-10
(2)	51	-18	-16	-12	-13
(3)	45.5	-35	-34	-32	-33

Table A.4 Summary of Computations of the Free Energy of Hydrolysis Reactions Considered in the Fe^{3+}—H_2O System

Reaction	$\Delta G°(T)$, Cal at Indicated Temperatures				
	298°K	333°K	373°K	423°K	473°K
(1)	-2550	-4774	-6621	-9295	-11880
(2)	-2500	-4250	-6185	-8598	-10859
(3)	4700	3176	1585	-250	-1826

Appendix B

X-RAY DIFFRACTION RESULTS

Appendix B

Table B.1 X-ray Diffraction Patterns of Goethite Using the Fe K_α Radiation

Reported		Sample	
d° Å	I/I_1	d° Å	I/I_1
5.0	20	4.92	30
4.21	100	4.29	100
3.37	20	-	-
2.69	80	2.87	75
2.57	20	-	-
2.48	20	2.71	100
2.44	70	2.65	65
2.25	20	-	-
2.18	40	2.44	40
1.719	50	-	-

Table B.2 X-ray Diffraction Patterns of Hematite Using the Fe k_α Radiation

Reported		Sample ($FeCl_3$ Leach)		Sample ($FeCl_3$/HCl	
d°A	I/I^+	d°A	I/I_1*	d°A	I/I_1*
3.66	25	3.92	50	3.81	50
2.69	100	2.89	100	2.88	90
2.51	50	2.72	100	2.72	100
2.201	30	2.45	35	2.45	40
1.838	40	2.16	40	2.16	40
1.690	60	2.06	60	2.06	60
1.596	16	2.01	16	2.01	16
1.484	35	1.96	35	1.96	35
1.452	35	1.95	35	1.95	35

+ Relative visual intensities, powder camera, CoK_α radiation

* Relative diffractometer peak heights

Table B.3 X-ray Diffraction Patterns of Chromite Using Fe K_α Radiation

Reported		Magnetic Particles	
d°A	I/I_1 +	d°A	I/I_1 *
4.82	50	4.92	10
2.95	60	3.12	40
2.52	100	2.73	100
2.40	10	-	-
2.07	70	2.34	70
1.69	40	2.06	40
1.60	90	2.0	90

\+ Relative visual intensities, powder camera, MoK_α radiation

* Relative diffractometer peak heights.